Processes Controlling Thermal Regimes of Secondary Channel Features in a Large, Gravel-bed River, Willamette River, Oregon, USA

Carolyn Gombert[1], Stephen Lancaster[2], Rebecca Flitcroft[3], and Gordon E Grant[4]

[1]US Army Corps of Engineers
[2]Oregon State University
[3]US Forest Service, Pacific Northwest Research Station
[4]USDA Forest Service, Pacific Northwest Research Station

November 23, 2022

Abstract

The thermal regime of rivers plays a key role in aquatic ecosystem health. In the Willamette River, OR, main channel temperatures can be too warm for cold water fishes, causing fish to concentrate in secondary channel features including side channels, ponds, and alcoves. However, temperature regimes vary among and within features. Improved understanding of physical processes controlling thermal regimes in gravel-bed rivers is needed for targeted conservation action. This study characterized thermal regimes on the Willamette through field observations of temperature continuously measured at one side channel, eight alcoves, and six beaver ponds over a two month period. Insight into these measurements was provided by two dimensionless quantities. The Richardson number, characterizing stratification, was calculated with temperature and flow data. Values showed two well-mixed sites and 13 stratified sites. Stratification allowed calculation of the hyporheic-insolation number, characterizing the ratio of cooling flux from hyporheic discharge to heat transfer from incoming solar radiation. As calculated hyporheic-insolation numbers for sites increased, measured temperatures at sites decreased, showing a bin-averaged logarithmic fit R2=0.97. Results further indicate secondary channel features that provide cold water habitat are characterized by stratification and cool hyporheic discharge. Stratification is a necessary yet insufficient condition for cold water to provide habitat for aquatic biota because cold areas may still be anoxic, as suggested by dissolved oxygen point measurements. The hyporheic-insolation number has the ability to predict and thereby classify the thermal regimes of secondary channel features based on minimal field measurements and could guide floodplain restoration efforts.

Processes Controlling Thermal Regimes of Secondary Channel Features in a Large, Gravel-bed River, Willamette River, Oregon, USA

C.E. Gombert[1], S.T. Lancaster[2], R.L. Flitcroft[3], and G.E. Grant[3]

[1]US Army Corps of Engineers, Sacramento, CA, USA.

[2]College of Earth, Ocean, and Atmospheric Science, Oregon State University, Corvallis, OR, USA.

[3]USDA Forest Service, Pacific Northwest Research Station, Corvallis, OR, USA.

Corresponding author: Carolyn Gombert (Carolyn.E.Gombert@usace.army.mil)

Key Points:

- Flow velocity and geomorphic history control water temperature in secondary channel features on gravel-bed rivers
- Off-channel features providing cold water habitat are characterized by stratification and long, high-permeability subsurface flow paths
- Cold water habitat locations on a floodplain can be predicted remotely using aerial photographs, public data sets, and literature values

Key Words:

Water temperature, off-channel habitats, hyporheic flow path, geomorphic change, heat budget, dimensional analysis

Suggested Indices:

Geomorphology: fluvial (1825, 1625)

Surface water quality (1871)

Energy budgets (1814)

River channels (1856, 0483, 0744)

Numerical approximations and analyses (1849, 3333)

Abstract

The thermal regime of rivers plays a key role in aquatic ecosystem health. In the Willamette River, OR, main channel temperatures can be too warm for cold water fishes, causing fish to concentrate in secondary channel features including side channels, ponds, and alcoves. However, temperature regimes vary among and within features. Improved understanding of physical processes controlling thermal regimes in gravel-bed rivers is needed for targeted conservation action. This study characterized thermal regimes on the Willamette through field observations of temperature continuously measured at one side channel, eight alcoves, and six beaver ponds over a two month period. Insight into these measurements was provided by two dimensionless quantities. The Richardson number, characterizing stratification, was calculated with temperature and flow data. Values showed two well-mixed sites and 13 stratified sites. Stratification allowed calculation of the hyporheic-insolation number, characterizing the ratio of cooling flux from hyporheic discharge to heat transfer from incoming solar radiation. As calculated hyporheic-insolation numbers for sites increased, measured temperatures at sites decreased, showing a bin-averaged logarithmic fit R^2=0.97. Results further indicate secondary channel features that provide cold water habitat are characterized by stratification and cool hyporheic discharge. Stratification is a necessary yet insufficient condition for cold water to provide habitat for aquatic biota because cold areas may still be anoxic, as suggested by dissolved oxygen point measurements. The hyporheic-insolation number has the ability to predict and thereby classify the thermal regimes of secondary channel features based on minimal field measurements and could guide floodplain restoration efforts.

1 Introduction

Water temperature is a key driver of biological processes in aquatic ecosystems (Cassie, 2006, e.g.), shaping species presence and distribution (Vannote et al., 1980). At different locations within a river, water temperature varies on both daily and annual bases (Johnson, 2004; Stefan & Preud'homme, 1993; Ward, 1985). Such patterns in thermal variability comprise a river's thermal regime and translate into phenological adaptation by native fishes, influencing processes such as metabolism, growth rate, reproductive success, and migration (Brett, 1971; Elliott & Hurley, 1997; Keefer & Caudill, 2015). Water temperature is thus a key water quality metric for riverine systems.

Thermal regimes vary systematically along a river and its floodplain (Steel et al., 2017). In areas with slowly moving water, such as stagnant pools, temperature varies with depth (Merck & Neilson, 2012). In some complex river-floodplain systems, such as the Tagliamento River in Italy, longitudinal variations in water temperature along the main channel are smaller than lateral variations in water temperature across the floodplain (Arscott et al., 2001). In smaller streams, narrow channel widths and forested canopies can prevent incoming solar radiation from significantly increasing water temperature (e.g., Beschta & Taylor, 1988; Johnson, 2004; Johnson & Jones, 2000). However, in larger rivers, greater channel widths are unlikely to be in full shade, particularly during midday, and the influence of riparian shading on water temperature is smaller (Poole & Berman, 2001). Furthermore, given water's large heat capacity and a main channel's large volumetric flow rate, inputs from groundwater and the hyporheic zone may only alter the water temperature of a mainstem by a fraction of a degree Celsius (Burkholder et al., 2008).

A balance of heat transfers determines water temperatures across a river-floodplain system (Figure 1a), and both physical principles and data suggest a hierarchy among heat transfer mechanisms in terms of their control on temperature. Moreover, this hierarchy of control varies according to time, location, and scale. At the scale of the stream network, shortwave solar radiation, or insolation, dominates heat input; when zoomed into a main channel cross-section, advection and dispersion dominate the local heat budget; at the scale of a floodplain pond observed at night, longwave, thermal radiation from the water surface may be the dominant heat transfer mechanism.

In streams that support habitat for cold-water fishes, water temperature and heat present a challenging water quality issue. Changes in mainstem temperature require subtractions of heat in proportion to discharge (400 MW/^{o}C for 100 m^3/s) and efforts required to bring larger rivers into compliance with regulatory standards may approach or surpass what is feasible in any reasonable regulatory regime. Already, studies have shown that the large heat capacity of water and large flow rates in the main channel of a large river limit the effect of heat transfer mechanisms tending to reduce water temperature, such as shade from riparian vegetation and cool-water inputs from groundwater and the hyporheic zone (Burkholder et al., 2008; Cluis, 1972; Johnson, 2004). However, such mechanisms may play significant roles in the heat budgets of secondary channel features, where the volumes and flow rates of water are typically much smaller, channels often much narrower, and the fraction of water surface area shaded by riparian vegetation potentially larger. Such secondary features include alcoves, features that are connected to the main channel only at their downstream end, and side channels, features connected to the main channel at both their upstream and downstream ends.

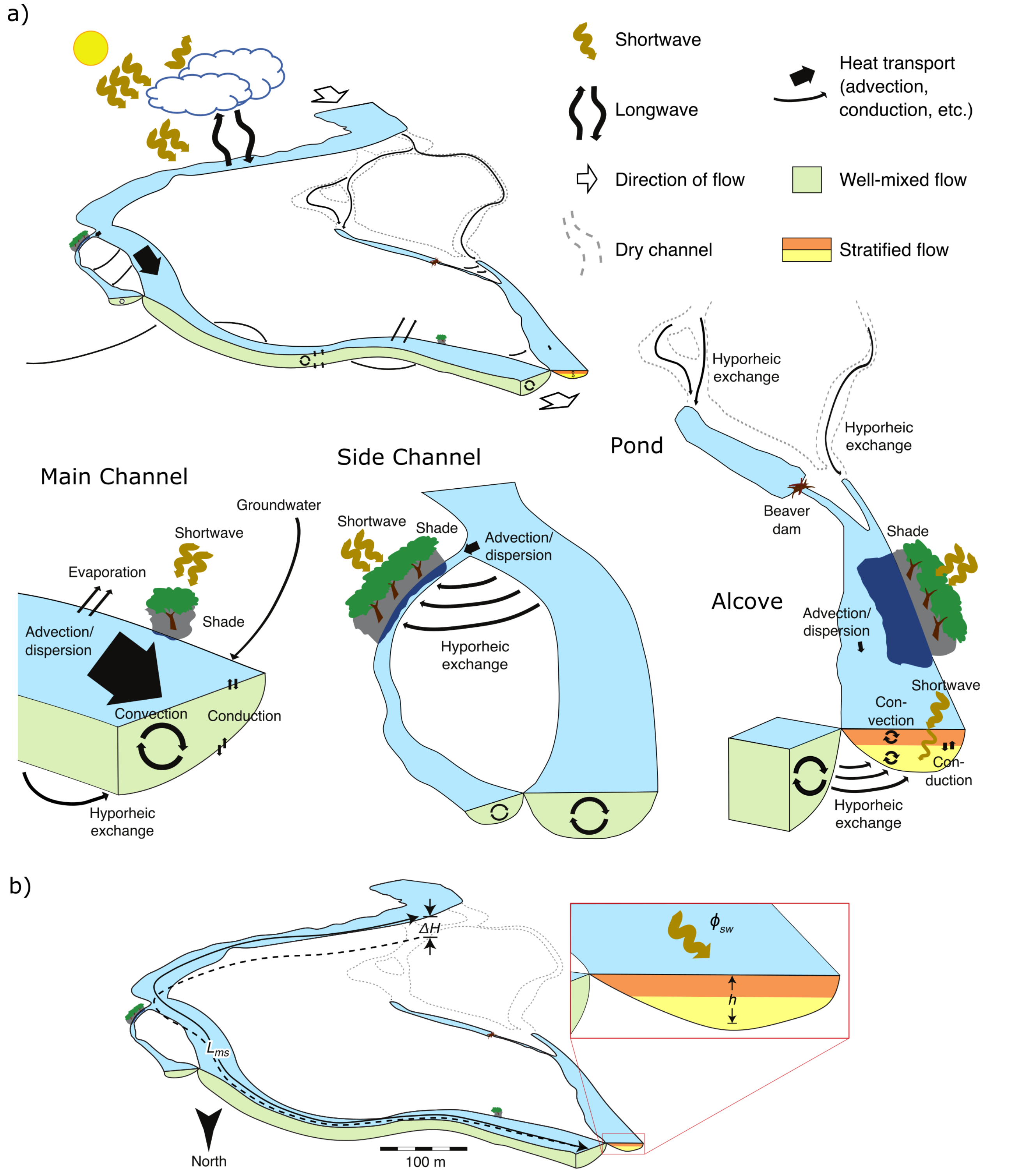

Figure 1. Schematic diagram, based on an oblique aerial photograph of the Willamette River, Oregon, of the heat budget (a) and key variables in dimensional analysis (b). Sections are colored to illustrate temperatures, where yellow is cold, orange is hot, and light green is intermediate. Black arrows indicate directions and relative magnitudes of heat fluxes. (a) In water bodies with large enough flow velocities, advection and dispersion dominate local heat transport and, with convective mixing, make water temperature nearly uniform; bare-gravel surfaces are abundant, and channel banks may have sparse riparian vegetation, which shades relatively little of wide channels. In ponds and alcoves cut off from surface flow, stratification into shallow and deep layers prevents mixing, and results in attenuation of shortwave radiation to deep layers, where hyporheic inputs may therefore dominate temperature. (b) Key variables in dimensional analysis include shortwave radiation, ϕ_{sw}, mainstem length, L_{ms}, and change in head along the hydraulic flow path, ΔH.

A potential management strategy is to shift away from emphasis on regulatory compliance in the mainstem towards a focus on cold-water refuges within a floodplain (Fullerton et al., 2018; Isaak, 2015; Torgenson et al., 2012). In this case, robust tools for predicting locations and quantities of cold water habitat are needed. While advances have been made in the area of temperature measurement tools, including networks of remote temperature loggers (e.g., Jackson et al., 2016) and remote sensing techniques (e.g., Dugdale, 2016), the development of predictive tools to estimate the location and proportion of available cool water habitats remains incomplete. In part, such development has been hindered by the fact that physical processes controlling river temperature heterogeneity remain difficult to isolate (Hannah and Garner, 2015). In the case of physically based deterministic models, outputs for predicted river temperatures are often limited by the quality and resolution of data. Furthermore, analytical models that may capture primary effects are unable to represent subtler secondary effects. For example, the Heat Source model used by the state of Oregon's Department of Environmental Quality is appropriate only for predicting time-varying temperature along the single spatial dimension of downstream distance. Even if hyporheic inputs could be adequately parameterized for use in this model, it assumes full lateral and vertical mixing and therefore cannot predict the effects of stratification of slowly moving water. The US Army Corps of Engineer's CE-QUAL-W2 model is two-dimensional and can therefore predict the effects of stratification, but still requires characterization of hyporheic inputs (Cole & Wells, 2006).

In an effort to elucidate the physical processes driving observed thermal heterogeneity in rivers and to address the need for predictive models for stream temperature, this study addresses the overarching question: What controls the thermal regime of secondary channel features in a large, gravel-bed river? Specifically, can we establish a physics-based framework that discriminates among features with different temperature regimes without requiring detailed examination, e.g., via deploying monitoring wells and modeling mass and heat transport in the subsurface and surface environments? While it has been established that alcoves and side channels provide critical ecosystem services for cold water anadromous fishes (e.g., Chinook salmon, cutthroat trout) requiring cool-water refuges during the summer (e.g., Isaak et al., 2015), prior studies of stream temperature, particularly of temperatures in off-channel water bodies, have not established a reliable framework for predicting those temperatures. Prior work has also provided some understanding of controls on temperature in a limited number of case studies, but these studies represent a large investment of resources, and the cases represent a small fraction of the total number of off-channel features (e.g., Fernald et al., 2006; Wallick et al., 2013). To address these gaps, this study seeks to explore the ways in which field measurements can be incorporated into a physically based framework to identify key drivers of water temperature in secondary channel features, with the ultimate goal of improving predictive capacity.

2 Conceptual Framework

Our conceptual framework seeks to establish a hierarchy of control for heat transfer mechanisms observed in secondary channel features. We build on the relative magnitudes of heat fluxes illustrated in Figure 1a, focusing specifically on heat transfer by advection/dispersion, shortwave radiation, and hyporheic exchange. We posit that secondary channel features with cool water will require: (a) inflow of cool water through the bed from the hyporheic zone, (b) reduction of heating by insolation through shading by vegetation or attenuation beneath a given depth of water, and (c) stratification, which is necessary to prevent mixing, i.e., advection/dispersion, between layers of warm, near-surface water heated by insolation and cool, near-bed water sourced by hyporheic flow. Our approach to evaluating this framework involves first determining presence of stratification, or dynamic stability. Then, for features where stratification is present, estimating the relative magnitudes of both cooling via hyporheic flow as well as heating via insolation, with the understanding that the latter may be reduced by shading and attenuation in the water column.

2.1 Stratification as Referenced by the Richardson Number

Thermal stratification in a water column occurs when lower density warm water sits above higher density cold water. Stratification can be quantified with the Richardson number, which, borrowed from the atmospheric, oceanic, and lacustrine sciences, is defined as the ratio of destruction of turbulent kinetic energy by buoyant forces and the production of turbulent kinetic energy by shear forces. Neglecting the small correction for the compressibility of water, the gradient Richardson number for layers is

$$\mathbb{R}i = -\frac{\frac{g}{\bar{\rho}}\frac{\Delta\rho(T)}{\Delta z}}{\left(\frac{\Delta u}{\Delta z}\right)^2} \quad (2)$$

where g is acceleration due to gravity (m/s^2); $\Delta\rho(T)$ is the difference in density of water (kg/m^3) between layers, calculated as a function of the water temperature, T (K), in each layer; Δz is the difference in height above the bed (m) between layers; Δu is the difference in time-averaged, downstream flow velocity (m/s) between layers; and $\bar{\rho}$ is the average density across layers (kg/m^3) (Peixoto & Oort, 1992). Flow is stratified for $\mathbb{R}i > 0.25$.

We calculated the Richardson number at sites where velocity measurements were obtained directly and used published values for density variation with temperature (Rumble, 2018). We tested temperature gradient as a proxy to assess stratification in all study sites because we did not obtain velocity measurements for all secondary channel features. Our proxy for the Richardson number, then, can be defined as,

$$\mathbb{R}i_p = \frac{\Delta T}{\Delta z} \qquad (3)$$

2.2 Cooling vs. Heating as Referenced by the Hyporheic-Insolation Number

To assess the relative magnitudes of cooling by hyporheic inflow and heating by insolation, we used dimensional analysis to derive a dimensionless ratio, a hyporheic-insolation number. Hyporheic flow is river water that enters sub-aqueous streambed sediments beneath or near the channel (i.e., the hyporheic zone), flows down-gradient, and reemerges into the river or off-channel water bodies. As hyporheic water travels along its flow path, dispersion in the subsurface attenuates temperature oscillations that are present when the river water enters the hyporheic zone. When compared to main channel temperature cycles, hyporheic zone cycles can be buffered (i.e., a difference in range) or lagged (i.e., a difference in phase) on either a diel or an annual period, as determined by hyporheic flow path length, hydraulic gradient, and hydraulic conductivity (Arrigoni et al., 2008; Burkholder et al., 2008). A shorter flow path, for example, may have a hyporheic temperature cycle lagged by 12 hours, discharging water that, relative to the main channel, is cooler during the day but warmer at night. Longer subsurface flow paths, however, may operate on an annual period corresponding to greater attenuation. In the summer, hyporheic flow reemerging will be consistently cooler than water in the main channel. Yet in the winter, it will be consistently warmer.

The magnitude of the hyporheic "cooling" flux per bed area can be represented as $\phi_{hr} = \rho c_w q_h \Delta T_h$ (W/m^2), where c_w is the specific heat capacity of water (J/kg K), q_h is unit hyporheic discharge (m/s), and ΔT_h is the difference between mainstem and hyporheic water temperatures (K). Assuming linear dispersion, that difference increases as $\Delta T_h \sim \sqrt{t_r}$, where t_r is the residence time of water in the hyporheic zone (s). As the residence time approaches the annual period, hyporheic water temperature should approach the mean annual water temperature in the main channel. For the purposes of dimensional analysis, then, we let $\Delta T_h \longrightarrow T_a\sqrt{t_r/t_a}$, where T_a is mean annual stream temperature (K), and t_a is the annual period (s). Residence time is $t_r = n\Delta x/q_h$, where n is porosity, and Δx is the length of the subsurface flow path. The hyporheic flow rate, q_h, is given by Darcy's law: $q_h = K\Delta H/\Delta x$, where K is hydraulic conductivity (m/s), and ΔH is the change in head along the hyporheic flow path (m).

Relative to the main channel, the water surface gradient in secondary channel features is effectively flat. The discharge in alcoves, predominantly sourced by subsurface flow, is much less than in the main channel, but alcove dimensions, especially near their mouths, are similar to those of the main channel. Therefore, flow velocities are small, ~10^{-2} m/s. Ponds are effectively perched alcoves and have similar flow velocities. Furthermore, when river stage of the mainstem is low, which is a condition that occurs in the Pacific Northwest rivers during the summer, flow velocities near the mouths of side channels are also much slower than in the main stem, ~10^{-1} m/s. For all of these secondary channel features, then, we estimate the difference in head along the hyporheic flow path as the product of mainstem water surface gradient, S_0, and length, L_{ms}, or $\Delta H = S_0 L_{ms}$. For alcoves (or side channels), mainstem length is the streamwise distance from the head of the dry (or submerged) channel head and the mouth, where it rejoins the main channel (Figure 1b). For ponds, that length is estimated according to the relative location of the downstream end of the pond. With all of the above substitutions and omitting porosity ($\sqrt{n}\sim 1$), we represent the magnitude of hyporheic cooling as

$$\phi_{hr} \sim \rho c_w T_a \sqrt{K S_0 L_{ms}/t_a} \qquad (4)$$

which preserves the original dimensions of heat flux per unit area (W/m^2)

The insolation heat flux per bed area can be represented as, $\phi_i = (1-\theta_s)e^{-\zeta h}\phi_{sw}$, where θ_s is the shaded fraction; ζ is the attenuation coefficient of light in water (1/m); h is depth below the water surface (m); and ϕ_{sw} is the incoming solar radiation per unit area (W/m^2). Preliminary sensitivity analysis of the influence of shade from riparian vegetation suggested θ_s could be omitted. Accordingly, we represent the ratio of cooling by hyporheic inflow and heating by insolation with a dimensionless ratio,

$$\frac{\phi_{hr}}{\phi_i} \sim \mathbb{H}_{ri} \equiv \frac{\rho c_w T_a}{e^{-\zeta h}\phi_{sw}} \sqrt{\frac{K S_o L_{ms}}{t_a}} \tag{5}$$

where $\mathbb{H}_{ri}$ is termed the hyporheic-insolation number.

Larger values of $\mathbb{H}_{ri}$ should correspond to greater effects of hyporheic cooling relative to heating by insolation. As greater hyporheic cooling (i.e., maximum "buffering") is associated with longer residence times in the subsurface, we expect that dispersion will lead to hyporheic inflow temperatures approaching the annual mean stream temperature as subsurface residence times approach a period of one year. Our metric for comparison with the hyporheic-insolation number therefore uses the annual mean stream temperature as a reference point: Locations with greater values of $\mathbb{H}_{ri}$ should have maximum daily temperatures more similar to the annual mean. That is, we expect an inverse relationship between hyporheic-insolation number and the difference between daily maximum temperature and the annual mean, $\Delta T_{sa} = T_{s,max} - T_a$, where $T_{s,max}$ is daily maximum temperature at a location, and T_a is the annual mean temperature in the main channel.

3 Methods

3.1 Study Area: Upper Willamette River, Oregon

Data collection took place on the upper Willamette River, a large, gravel-bed river in northwestern Oregon, USA (Figure 2). The river flows from south to north through a wide, structural valley bounded on the east by the Cascade Range and on the west by the Oregon Coast Range. Specifically, the study area comprised two reaches of the upper Willamette River. The

Harrisburg reach, located upstream of USGS gage 14166000 at Harrisburg (river km 199.5), has a contributing area of 8,860 km^2. The Corvallis reach, located upstream of USGS gage 14171600 at Corvallis (river km 165.7), has a contributing area of 11,400 km^2. The average stream gradient of 0.98 m/km along the Harrisburg reach is steeper than the gradient of 0.62 m/km along the Corvallis reach (Dykaar & Wigington, 2000). A mean annual flow of 330 m^3/s (11,600 ft^3/s) occurs at the Harrisburg gage while a mean annual flow of 370 m^3/s (13,100 ft^3/s) occurs at the Corvallis gage (Table 1).

The banks of the upper Willamette are predominately comprised of erodible Holocene alluvium which is set atop older Pleistocene deposits. The Pleistocene units consist of partially cemented gravel and a top set of weathered silt, which is itself overlaid with rhythmically bedded Missoula flood deposits composed of both weathered silt and clay (O'Connor et al., 2001). The partially cemented Pleistocene terrace is 2 to 5 times more resistant to bank erosion than the Holocene alluvium (Wallick et al., 2006).

Within the erodible Holocene alluvium floodplain, the upper Willamette is dynamic and typically has multiple threads along a significant fraction of its length, especially in the reaches with unreinforced banks on both sides of the river (<25%; Wallick et al., 2007). The U.S. Army Corps of Engineers operates eight flood-control dams upstream of Harrisburg, nine upstream of Corvallis. At the USGS 14174000 gage at Albany (the nearest with a long enough record), the mean annual flood discharge was 3240 m^3/s prior to flood control (WY 1893–1941) and 1840 m^3/s after (WY 1973–2019); mean annual flood stage dropped by 2.0 m. In the present regime of flood control, high flows still lead to changes in the channel planform, although those changes are less frequent and dramatic than before flood control. The dynamic quality of the upper

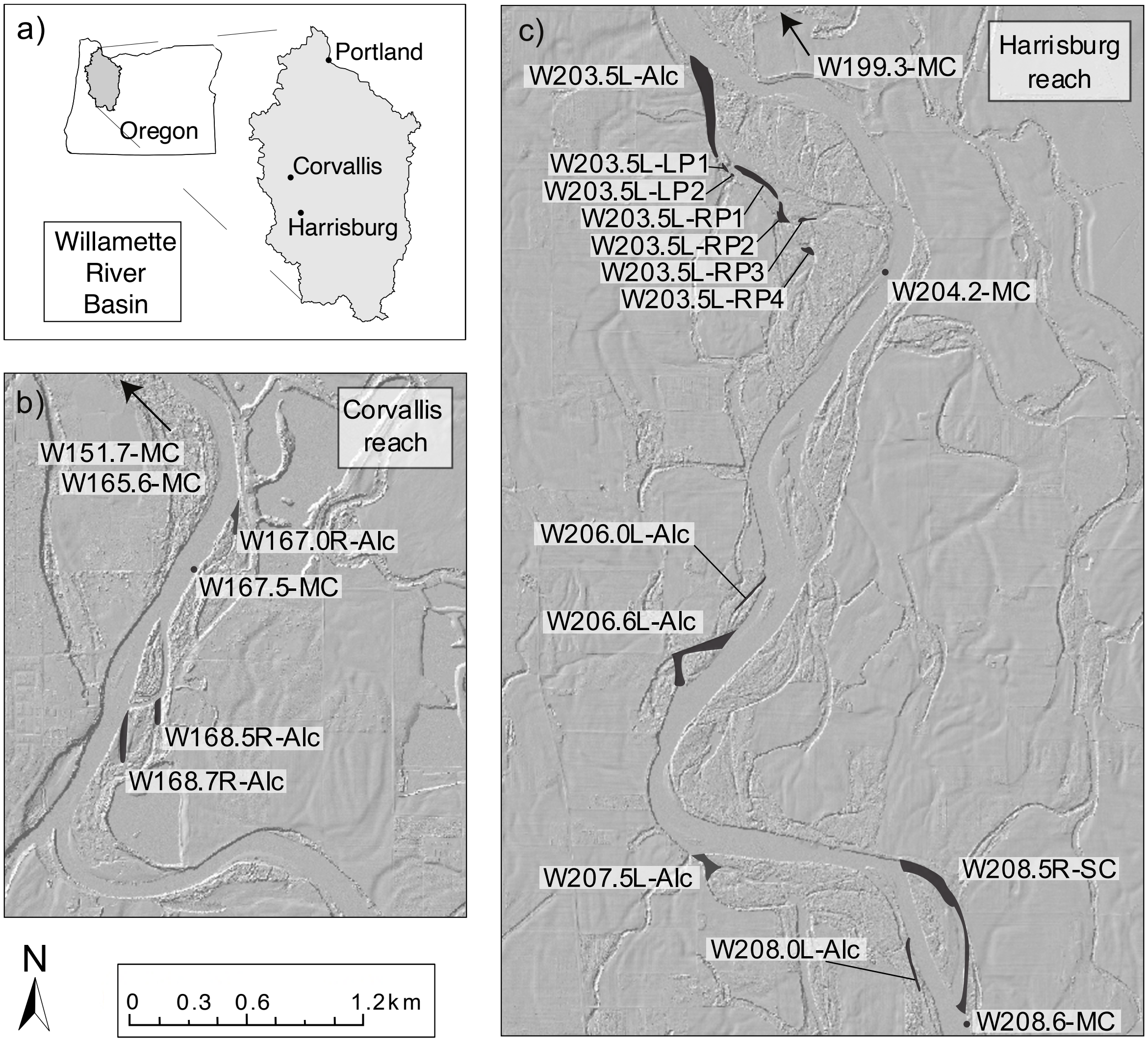

Figure 1. The study area is located in the Willamette River basin (a) and comprises the Harrisburg (b) and Corvallis (c) reaches. Off-channel sites, including eight alcoves, six ponds, and one side channel, are masked in dark gray; mainstem site locations are indicated with dark gray circles; all sites are labeled. Downstream locations of Harrisburg (b), Corvallis, and Albany gages (c) are indicated with arrows and labels using the same naming convention as the study sites (see text).

Willamette River continues to allow for the creation of new secondary channel features such as the alcoves, side channels, and ponds instrumented in this study.

The climate of the upper Willamette Valley is characterized by cool, wet winters, and dry, warm summers. Average annual precipitation in the upper Willamette Valley is 162 cm (USGS StreamStats) and falls predominantly as rain during the period from October through June. Summer flow in the upper Willamette is predominantly from springs in the Cascade Range and from reservoirs, which are managed in the summer to increase discharge and thereby mitigate high stream temperatures. Daily maximum stream temperatures at the Harrisburg gage typically exceed the regulatory standard of 18 ^{o}C from mid-July to mid-August, and even daily minimum temperatures exceed the standard for much of that time (ODEQ, 2007).

3.2 Field Measurements

The goal of measurements and observations in the field was to characterize thermal regimes in secondary channel features, including side channels, alcoves, and ponds, within the area defined by the modern floodplain of the upper Willamette River. Concurrent measurements in both secondary channel features and the main channel allowed for characterization of temperatures in the secondary channel features relative to temperatures in the main channel.

In general, we define secondary channel features in the study as follows: Side channels are features that are connected, with no discontinuity, to the main channel at both their heads, where flow is diverted from the main channel, and at their mouths, where flow rejoins the main channel. Side channels carry less than half of the total discharge of the river, typically much less, and usually have riffles at their heads. Alcoves, on the other hand, are off-channel water bodies with only one connection to the main stem, almost always at the downstream end. An alcove may develop when aggradation occurs at the upstream end of a side channel, causing the flow of surface water at the feature's head to cease. Additionally, depending on the stage of the main channel, a feature that is a side channel at high flows, i.e., connected at its upstream and downstream ends, may become an alcove at lower flows, with the former side channel's upstream riffle becoming exposed, and all water entering the current alcove head through the hyporheic zone rather than from an upstream surface water connection. Along the upper Willamette, some alcoves occur on a former channel path that also includes ponds, or stretches

Table 1. Reach Characteristics[a]

Gage location	USGS Gage ID	WRS[b] (km)	Contrib. area (km²)	Stream gradient[c]	Mean ann. water temp. (°C)	Max. water temp., 2017 (°C)	Chan. width[d] (m)	Mean ann. flood disch. (m³/s)	Min. disch., 2017 (m³/s)	MAF – min. 2017 stage (m)
Harrisburg	14166000	199.3	8860	0.098%	11.4	20.7	181	1520	119	3.12
Corvallis	14171600	165.6	11,400	0.062%	12.3[e]	22.4	145	1840	123	5.14

[a] From Harrisburg and Corvallis gages: Mean ann. water temp. = mean of temperature measurements recorded at 15-minute intervals during calendar year 2017; Max. water temp., 2017 = maximum of 15-min. temperature data for summer 2017; Mean ann. flood disch. = mean of annual peak discharge records for gage for water years (WY) 1973–2019 (Harrisburg) and WY 2010–2019 (Corvallis); Min. disch., 2017 = minimum of discharge measurements recorded at 15-min. intervals during summer 2017; MAF – min. 2017 stage = difference between stage of mean annual flood and low stage in summer 2017.
[b] Willamette River Slices from Hulse et al., 2002
[c] Dykaar & Wigington, 2001
[d] Wallick et al., 2007
[e] Temperature data from Albany gage (14174000) at WRS 151.7 km

of deep, flat water. Specifically, ponds are marked at their downstream mouths by a beaver dam and at their upstream heads with either another beaver dam or a connection to dry land (Figure 1). Note that all of the water in ponds and alcoves is sourced by hyporheic flow, even if that hyporheic flow emerges from the subsurface at some distance upstream of a particular pond or alcove.

3.2.1 Measurement Locations

Aerial photographs from May 2016 facilitated the identification of off-channel sites grouped within two study reaches along the upper Willamette River: Corvallis (Figure 2b) and Harrisburg (Figure 2c). The selected reaches were accessible and contained a diversity of secondary channel features, including side channels, alcoves, and beaver ponds. In total, 15 secondary channel features were instrumented. These off-channel sites included one side channel, eight alcoves, and six beaver ponds. Twelve of the off-channel sites, including the side channel and all of the beaver ponds, were located in the Harrisburg reach. The remaining three alcoves were located downstream in the Corvallis reach. In addition, instruments were deployed at three locations along the main channel. Two of the main channel deployments were located in the Harrisburg reach. One was located in the Corvallis reach (Figure 2b,c).

We adopted a naming convention in which sites were identified by feature type, bank location, and a river kilometer based on the Willamette River Slices ("W") Framework (Hulse et al., 2002). Feature types included side channels ("SC"), connected to the mainstem at both the upstream head and downstream mouth; alcoves ("Alc"), connected to the mainstem only at the downstream mouth; ponds ("P"), where beaver dams impounded water within abandoned channels on the floodplain; and the main channel ("MC"). Off-channel sites had either right-bank ("R") or left-bank ("L") locations identifying the river or alcove bank from which the feature originated, where right and left were determined with respect to the downstream direction. River kilometer numbers were assigned based on location of the upstream head for side channels, the downstream mouth at the confluence with the main channel for alcoves, the mouth of the downstream alcove for ponds, or the instrument itself for the main channel.

At the off-channel sites, a rangefinder (Nikon) and hip chain were used to measure the length of each secondary feature from its upstream terminus to its downstream mouth or dam in the case of beaver ponds. Based on these longitudinal measurements, instrumented columns were placed at head, midpoint, and mouth locations, at 15 m (±5m) downstream of the upstream terminus, equidistant between upstream terminus and mouth or dam, and 30 m (±10m) upstream of the actual mouth at the confluence with the mainstem or the dam, respectively (Figure 3a). Columns were located along the centerline in side channels and alcoves and along the thalweg in ponds. At each column, measurement stations were located at three elevations, i.e., bottom, middle, and top (Figure 3b), relative to the total water depth. If the total water depth was shallower than 0.45 m, stations were located at only two elevations, bottom and top. At the one side channel site, one column with two stations was located at the midpoint of the shallow channel crossing the riffle at the upstream end; in the deep water downstream of the riffle, three columns of three stations each were located, as in alcoves, at head, midpoint, and mouth (Table 2). Each mainstem site contained only a single station near one bank and at 0.15 m (±0.05 m) above the bed.

3.2.2 Temperature Measurements

From July through September 2017, Onset Hobo Tidbit v2 data loggers were deployed to measure and record water temperatures (±0.2 °C) at 15-minute intervals. At each of the 15 off-channel sites, the average deployment period for a particular configuration of measurement

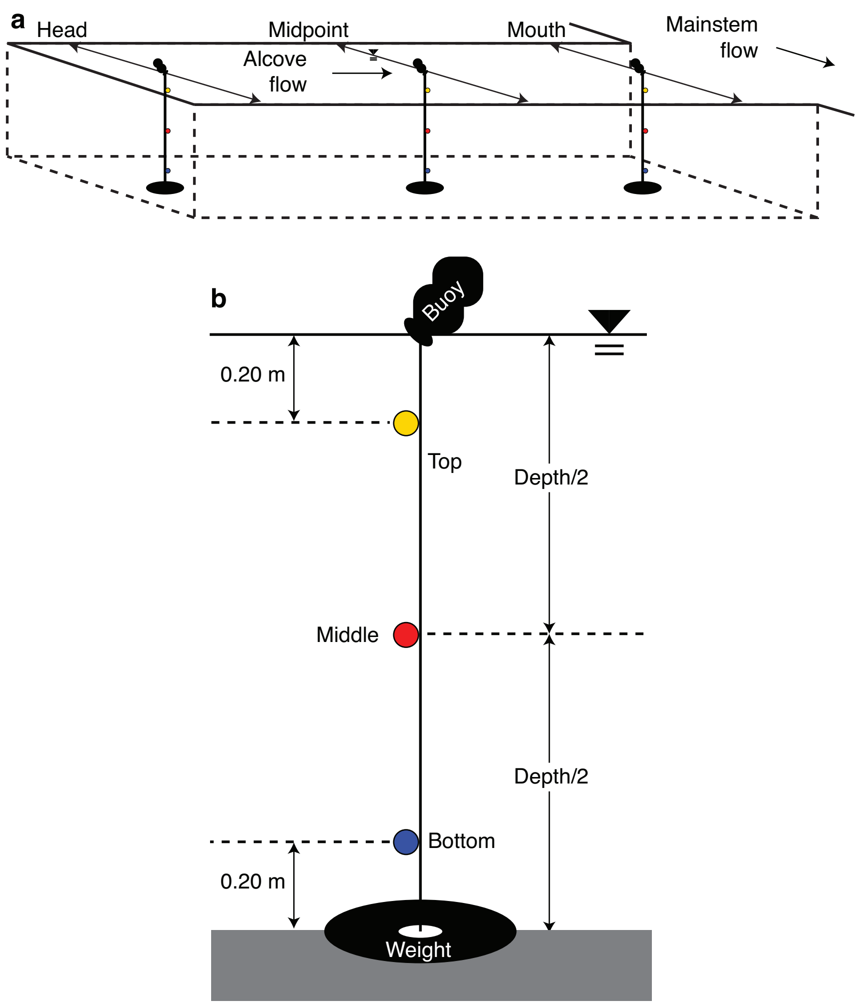

Figure 2. Temperature logger deployment scheme for off-channel sites: a) longitudinal positions of vertical columns at the head, midpoint, and mouth of secondary channel features, and b) vertical positions of loggers at three stations, bottom, middle, and top, along a cord suspended from a buoy and held in place by a weight (3 kg). Arrows indicate direction of flow in the main channel and in the side channel/alcove/pond.

Table 2. Summary of Measurements

	Dimensions		Temperature measurements							DO meas.		Flow measurements	
Site	Len. (m)	Avg. dep. (m)	No. stns.	No. cols.	Stns. per col.	Days of yr	Stn-days	Col-days	Site-days	Days of yr	No. stns.	Method	Days of yr
W167.0R-Alc	162	0.62	9	3	3	189–190	18	6	2				
W167.5-MC			1			189–226	38						
W168.5R-Alc	92	1.1	9	3	3	220–226	63	21	7	217	9		
W168.7R-Alc	187	1.3	9	3	3	192–197, 217–226	144	48	16	216	9		
			8	3	2/3/3	189–191, 198–216	176	66	22				
W203.5L-Alc	450	1.3	9	3	3	194–202	81	27	9			SD	201
			15	5	3	203–239	555	185	37	223	15	MM	201, 236
										236	15		
W203.5L-LP1	25	0.60	6	2	3	230–239	60	20	10	236	6		
W203.5L-LP2	10	1.4	3	1	3	230–236	9	3	3	236	3		
			6	2	3	237-239							
			8	3	3/2/3	248–251	24	8	4				
W203.5L-RP1	340	1.1	9	3	3	230–239	90	30	10	236	9		
W203.5L-RP2	100	2.4	9	3	3	230–243	126	42	14	236	9		
W203.5L-RP3	90	0.76	9	3	3	230–239	90	30	10	236	9		
W203.5L-RP4	50	1.8	9	3	3	245–254	60	20	10				
W204.2-MC			1			194–254	58						
W206.0L-Alc	146	0.82	9	3	3	200–204	45	15	5	205a	9	MM	205
										205b	9		
W206.6L-Alc	247	1.6	9	3	3	223–227	45	15	5	222	9	SD, MM	222
W207.5L-Alc	70	1.8	9	3	3	208–213	54	18	6	207	9	SD, MM	213
										214	9		
W208.0L-Alc	100	0.52	9	3	3	200–205	54	18	6	206a	9		
										206b	9		
W208.5R-SC	790	0.72	11	4	2/3/3/3	203–220	198	72	18	223	11	MM	202, 221
W208.6-MC			1			203–251	58						
Totals:							2198	668	201				

Len. = feature length; Avg. dep. = average depth at columns; No. stns. = number of stations at site; No. cols. = number of columns at site; etc.
Days of year = Calendar day: 181 = 6/30; 212 = 7/31; 243 = 8/31
DO = dissolve oxygen
Flow measurement methods: MM = Marsh-McBirney Flowmate 2000 with top-setting wading rod; SD = salt dilution with calibrated Onset HOBO U-24 conductivity-temperature loggers.

stations was 11 days, but varied from 2 to 37 days, where only days with instruments deployed from midnight to midnight are counted (Table 2). Whether deployments were long or short was effectively arbitrary. At the three mainstem sites, loggers were deployed for the entire duration of the study.

During the deployment period at each site, the temperature loggers were secured at all measurement stations, e.g., three columns of three stations each for a total of nine loggers at each off-channel site (Figure 3). This systematic deployment of loggers at each off-channel site facilitated estimation of the Richardson number (2) and its proxy (3) for layers represented by measurements at the top and bottom stations of each column. At each mainstem site, a single logger was secured by means of the buoy-weight (12 kg) method or by fastening a logger to the top of a cinder block (13.5 kg).

Including the mainstem sites, temperature measurements comprised more than 2000 "station-days," i.e., complete calendar days of measurements at a station (Table 2). Calculations of Richardson number (2) or temperature gradient (3) required at least two measurements in a column; for these purposes, measurements at the off-channel sites comprised more than 600 "column-days," i.e., complete calendar days of measurements at two or more stations in a vertical column (Table 2). It may be convenient to group all of the measurements for a particular configuration of stations at a site and on a calendar day into a "site-day," so that temperature measurements at off-channel sites comprised more than 200 site-days (Table 2).

3.2.3 Flow Measurements

We used a flow meter and salt dilution to measure discharge and flow velocity at five sites (Table 2). Each of these five sites exhibited shallow surface flow, e.g., over the riffle at the head of the side channel and into alcoves from upstream beaver ponds, with flow velocities great enough (≥0.15 m/s) to allow discharge measurement with a portable flow meter (Marsh-McBirney FlowMate 2000) and a top-setting wading rod (Table 2).

Whereas the flow meter was only useful at shallow parts of, or inflows to, secondary channel features, we used salt dilution to measure discharge and flow velocity in the deep channels at three of the alcove sites where we also used the flow meter (Table 2). If injected salt is well mixed over the width and depth of the channel, discharge is inversely proportional to the integrated conductivity relative to background. However, where stratification and slow flow prevent full mixing, flow velocity can still be estimated from the timing of the breakthrough curve at conductivity loggers at known distances downstream of the salt injection location. Prior to the salt injection, Onset HOBO U-24 conductivity-temperature (CT) loggers (±2 μS/cm), set to record every 10 seconds, were calibrated with a known mass of salt and water from the alcove and then secured at middle and bottom stations of columns downstream of the salt injection location. At W206.6L-Alc, CT loggers were secured at the middle stations of the three centerline columns. At the head and midpoint locations, four more CT loggers were secured at middle stations on additional columns placed on both sides of the existing centerline columns, halfway to either bank. Each salt injection used a known mass of salt (Morton Pickling Salt) dissolved in water from the alcove and then spread across the width of the alcove at its upstream end. Time of injection and distance to CT logger stations were recorded.

3.2.4 Dissolved Oxygen Measurements

Dissolved oxygen (DO) point measurements were taken at 13 of 15 off-channel sites (Table 2). Using a handheld YSI-ProODO probe (±0.1 mg/L), we measured temperature (°C) and DO (mg/L) at all stations at 13 sites (Table 2). DO readings were recorded from July 24 through August 24 (Table 2) between 9:00 and 15:00 PDT. Unlike the automatic temperature and conductivity measurements recorded by loggers at fixed positions, the DO measurements were recorded by manually lowering the probe to the appropriate water column depth and recording the reading on the digital meter once it had reached a stable value.

3.3 Estimation of Values for Dimensionless Numbers

All values used to calculate the Richardson number (2) or its proxy (3) were estimated from field measurements. However, of the ten values required for calculation of the hyporheic-insolation number (5), only one, i.e., water column depth, was measured at our sites in the field. All other values were estimated from public data sets, literature values, and publicly available aerial photographs.

For all five sites where velocity measurements were obtained, direct calculation of the Richardson number (2) was possible. We calculated a density gradient through comparison of temperatures recorded at two stations on the same column to published values of water density and temperature, interpolating between published data points where necessary (Rumble, 2018). In order to capture the greatest possible variation in temperature within the water column, measurements from the top station and the bottom station were used. Measurements taken at the time of the daily maximum temperature at the top station and the known heights of the stations yielded,

$$\frac{\Delta\rho}{\Delta z} = \frac{\rho(T_t) - \rho(T_b)}{z_t - z_b}$$

where T_t and T_b are temperatures recorded at top and bottom stations, respectively, and z_t and z_b are relative heights of the two stations, respectively.

We calculated the velocity differential from measured velocities and the no-slip boundary condition at the bed. For discharge measurements, average velocity for the cross-section at a column location is $U = Q/A$, where Q is discharge, and A is area of the cross-section. At off-channel sites where flow velocity was measured with a flow meter, Q and A values for a given lateral cross-section location are known. If we assume the average velocity for the cross-section is equal to the velocity at 0.4 × the total depth at the column, the velocity gradient is

$$\frac{\Delta u}{\Delta z} = \frac{U}{(0.4)z_c}$$

where z_c is the water depth at the column. For measurements of flow velocity from the timing of breakthrough curves, the velocity gradient is

$$\frac{\Delta u}{\Delta z} = \frac{L_c}{t_p z_s}$$

where L_c is the distance from the salt injection location to the column at which the breakthrough curve was detected; t_p is the time between injection and detection of the peak in conductivity; and z_s is the height of the station of the CT logger above the bed. Finally, we used $g = 9.81$ m/s^2 and $\bar{\rho} = 1000$ kg/m^3.

For off-channel sites without flow measurements, we used temperature measurements from the bottom and top stations on a column and the depth measurements to calculate the proxy for Richardson number (3). Similar to the calculations for the Richardson number, calculations for the proxy of temperature gradient used temperatures measured at the time of maximum daily temperature recorded at the top station in the column, so each column-day yielded one estimate of temperature or density gradient.

Values for the hyporheic-insolation number taken from public data sets include the mean annual stream temperature (T_a) and the incoming solar radiation per unit area (ϕ_{sw}). For our calculations, T_a was the average of mainstem temperature measurements recorded at 15-minute intervals for the calendar year 2017 at the USGS Harrisburg gage for the Harrisburg reach and the USGS Albany gage for the Corvallis reach, respectively (Table 1). Values for ϕ_{sw} were calculated from measurements at Oregon AgriMet Weather Station Corvallis location (crvo), where incoming solar radiation was recorded at 15-minute intervals. For comparison with water temperature recorded on a given calendar day, we calculated the average incoming solar radiation for the same given calendar day. In relation to our study area, the AgriMet Station is located approximately 17 km downstream of the Corvallis reach.

Literature values informed the quantities used for three variables in the hyporheic-insolation number. Stream gradient (S_0), hydraulic conductivity (K), and the attenuation coefficient (ζ) were each taken from published sources (Dodd & Wiles, 2010; Dykaar &

Wigington, 2000; Fernald et al., 2006; Squeochs, 2011). Stream gradients for both reaches were estimated by Dykaar and Wigington (2000) (Table 1). Hydraulic conductivity values were based on slug tests in the Harrisburg and Corvallis reaches (Fernald et al., 2006; Squeochs, 2011). Whereas Fernald et al. (2006) measured values on gravel bars with a range of apparent ages, we used aerial photographs from May 1994 and July 2000 to determine the relative age of each site. Sites within the flow path of the 1994 main channel were determined to be young, sites that were abandoned by the main channel and unvegetated were characterized as developing, and sites that were abandoned by the main channel and vegetated were classified as mature. Lastly, attenuation coefficient values were estimated from data collected for lakes in Oregon exhibiting oligotrophic, mesotrophic, and eutrophic conditions (Dodds & Wiles, 2010).

4 Results

Raw results comprised water temperature time series and point-in-time measurements of dissolved oxygen and flow. Ultimately, the temperature and flow data were reduced to values used in calculations of the Richardson number (2), its proxy (3), and the hyporheic-insolation number (5).

4.1 Thermal Regimes

Temperature measurements at all sites consist of more than 2000 station-days recorded at 15-minute intervals (Table 2). From August 1 to 3, 2017, a reservoir drawdown increased river stage by 0.5 m at the USGS Harrisburg Gage, and the elevated stage persisted through August. The averaged discharge for the week prior to the drawdown (July 25 through 31, 2017) was 120 m^3/s (4,300 ft^3/s) while the averaged discharge measurements for the week after the drawdown (August 4 through August 10, 2017) equaled 215 m^3/s (7,600 ft^3/s). The change in discharge, and the concomitant increases in water level, allowed data collection at sites before and after the change to cover a wider range of relevant conditions for evaluation of our hypotheses.

Selected time series shown in Figure 4 illustrate thermal regimes worthy of later discussion. The remaining records are available in the supporting information. A diel cycle of temperature fluctuations is evident at all stations (Figure 4), but amplitude and phase of fluctuation varied among sites, columns at a site, and, notably, stations on a column.

Temperature variations with depth were consistent with stratification at 13 sites, including all six ponds and seven of the eight alcoves. (Alcove W206.6L-Alc did not present temperature variations with depth.) Water temperatures were always coolest near the bed and warmest near the water surface. Near-surface temperatures fluctuated with larger amplitude than near-bed temperatures. At 11 of the apparently stratified sites, water temperatures increased with increasing distance downstream, as at W207.5L-Alc (Figure 4). However, at two stratified sites, W206.0L-Alc and W168.5R-Alc, water temperatures at bottom, middle, and top stations all decreased with increasing distance downstream (Figure 4).

Water temperatures were nearly uniform with depth at two sites, W208.5R-SC and W206.6L-Alc (Figure 4). At both sites, near-bed temperature measurements were within 0.5 °C of near-surface temperature measurements. Only one local exception was observed at the most downstream section of the deep side channel reach at low stage (Figure 4).

In the side channel and in the alcoves, daily minimum temperatures occurred in the morning between 08:00 and 09:00. Temperatures tended to peak in the late afternoon to early evening between 15:00 and 18:00. The time of daily maximum temperature varied with depth. For example, the peak temperatures recorded by the top and bottom loggers deployed at the head of W206.0L-Alc were offset by ~9 hours (Figure 4). The time of daily maximum temperature also varied with distance downstream. That is, the daily maximum temperatures at the head, the midpoint, and mouth did not always occur at the same time of day.

Compared to secondary channel features, the amplitude of the diel temperature cycle in the main channel is small. Mainstem temperatures at higher stage were generally cooler than at lower stage. At lower river stage, loggers in the main channel reached their maximum between 15:00 and 16:00 in the Harrisburg reach, and between 17:00 and 18:00 in the Corvallis reach. At higher river stage, maximum temperatures at Harrisburg occurred between 19:00 and 20:00, while the maximum in Corvallis remained between 17:00 and 18:00.

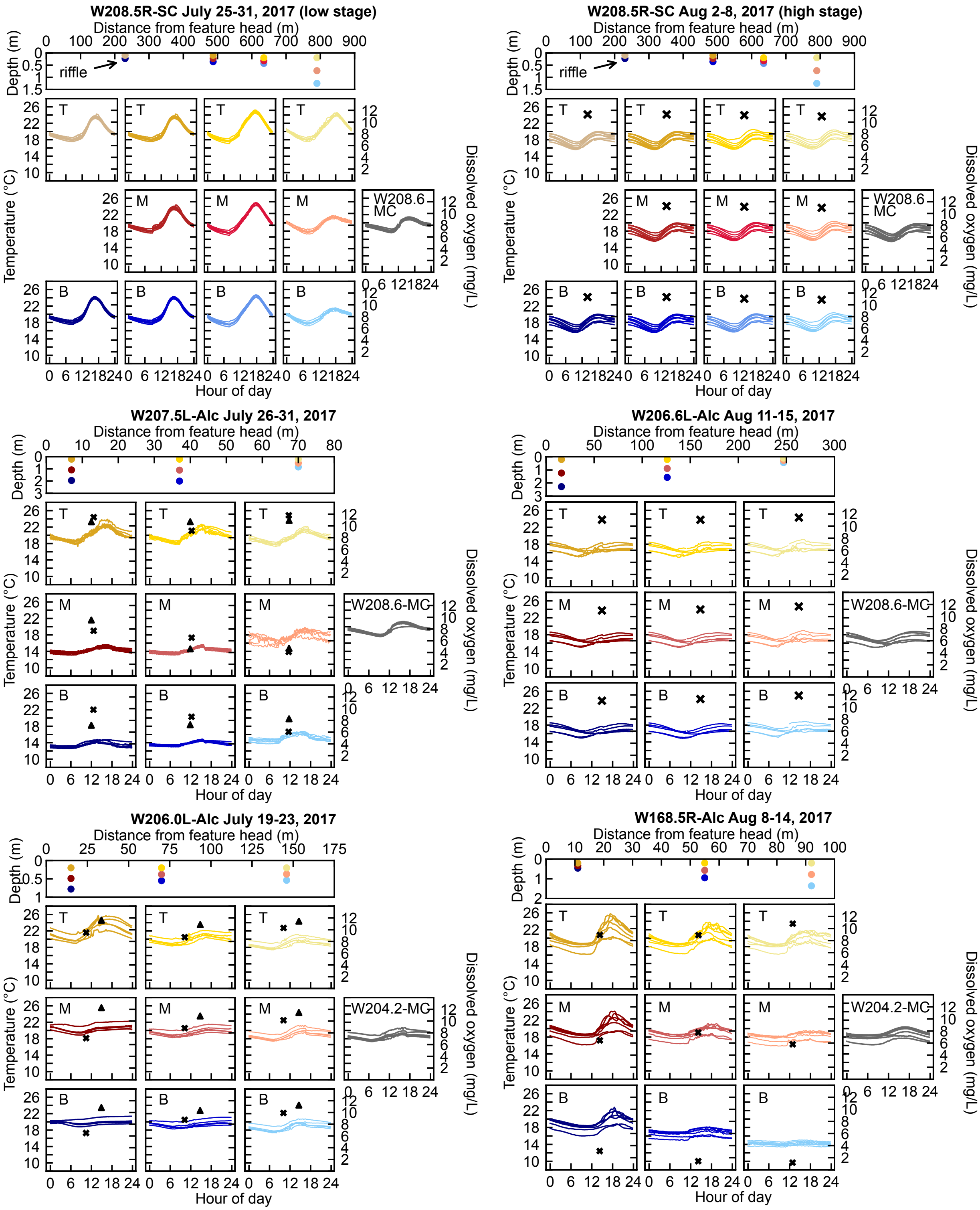

Figure 3. Water temperature (lines, left-hand y-axis) and dissolved oxygen ("x" or triangle, right-hand y-axis) vs. hour of day (x-axis), grouped by site and time period (site name and month/day of 2017 in group title), for up to 7 diel cycles each, for the side channel and four alcoves. All temperature and dissolved oxygen axes have the same scale. In each grouping, each graph corresponds to one station at the site, plus one graph for the same days at the mainstem site indicated on the graph (B = bottom, M = middle, T = top; Figures 2 and 3; Table 2). Depths of stations at each site are shown as well, plotted by distance from feature head. In total, 361 station-days at secondary channel features are shown.

4.2 Flow Measurements

Salt dilutions were unsuccessful in providing measurements of discharge, but some results did allow estimates of flow velocities. Two issues prevented calculation of discharge as a function of the integral of the conductivity relative to background. First, the method requires the salt plume to be fully mixed over the cross-section, and stratification in alcoves prevented this condition being met. Second, background conductivity in alcoves was highly variable in both time and space, and some background levels exceeded even the peaks due to salt injection. In a few cases, however, signals were discernable, and the timing of breakthrough curves provided estimates of flow velocities.

Velocities were estimated as follows. At W207.5L-Alc, measurement of discharge in an inflow channel with a flow meter yielded a minimum discharge estimate and, with cross-sectional area measured at the columns, velocities for the alcove. At W203.5L-Alc, travel time of peaks in conductivity after salt injection yielded velocity at low stage between the columns in the alcove's left fork and between the columns at the mouth of the left fork and midpoint of the main alcove. With cross-sectional area measured at the latter column as well as the column at the mouth, velocity at the mouth column was estimated. During low-stage, measurement of discharge in the right-fork inflow channel was small and made no significant contribution. At high stage in W203.5L-Alc, discharge measured in the right-fork inflow channel was added to discharge estimated in the left fork from low-stage velocities and cross-sectional areas, and velocity at the main alcove columns was estimated from that sum. At both low and high stages in W208.5R-SC, measurement of discharge with a flow meter at the riffle and head columns yielded velocities at those columns, as well as minimum discharge and, thus, velocity estimates for the midpoint and mouth columns. At W206.6L-Alc, travel times to all three columns from salt injection upstream of the head column yielded velocity estimates for each column. Discharge measured at the midpoint column of W206.0L-Alc, with cross-sectional areas, was used to estimate flow velocity at all three columns.

Discharge measured at two inflow channels to W206.6L-Alc revealed that their combined discharge (1.62 m^3/s) was similar in magnitude at high stage to the discharge in the channel connecting W208.5R-SC to the main channel (2.33 m^3/s). Closer inspection of the site, W206.6L-Alc, revealed that the emergent surface separating the alcove from the main channel was a log jam that permitted significant flow from the main channel, so that this alcove was more similar to the side channel, W208.5R-SC, than to the other alcoves.

4.3 Dissolved Oxygen in Secondary Channel Features

Dissolved oxygen levels were measured at 13 of the 15 study sites (the two sites with no measurements are W167.0R-Alc and W203.5L-PR4). In general, dissolved oxygen point measurements varied by depth and by distance downstream (Figure 4). At two sites, W208.5R-SC and W206.6L-Alc, dissolved oxygen point measurements were between 10.3 and 11.9 mg/L, and differences between readings taken at different depths were small, i.e., < 0.1 mg/L. The most downstream section of W206.6L-Alc was an exception, with a slightly larger difference, i.e., > 0.5 mg/L, between the near-bed and near-surface readings at the mouth of the feature.

At other alcoves, dissolved oxygen readings tended to show greater variation with depth, with differences upwards of 4 mg/L along the water column. Typically, levels of dissolved oxygen decreased with depth and increased with distance downstream. The lowest dissolved oxygen readings were taken at near-bed depths. The highest dissolved oxygen levels were recorded at the most downstream end of each feature at near-surface stations.

4.4 Dimensionless Numbers

4.4.1 Richardson Number Describes Stratification in Secondary Channel Features

Values of Richardson number were calculated for sites where flow velocities were measured, including the side channel and four alcoves. Richardson numbers for a given column-day were graphed with temperature gradient for the same column-day in order to assess the temperature gradient alone as a proxy indicator of stratification (Figure 5). That is, Richardson number effectively contains temperature gradient in that the density gradient is a function of the top and bottom temperature measurement of each column-day, but small temperature gradients can result in stratification for small enough flow velocities. Indeed, the results show that temperature gradients in stratified and mixed column-days overlap in the range 0.5 to 3.5 °C/m. In general, column-days in alcoves were stratified, and column-days in the side channel were mixed. The exceptions are as follows: first, all column-days in W206.6L-Alc were mixed, i.e., had $\mathbb{R}i < 0.25$; and second, at low stage, i.e., prior to the reservoir release beginning August 1, all column-days at the mouth of W208.5R-SC were stratified, i.e., $\mathbb{R}i > 0.25$.

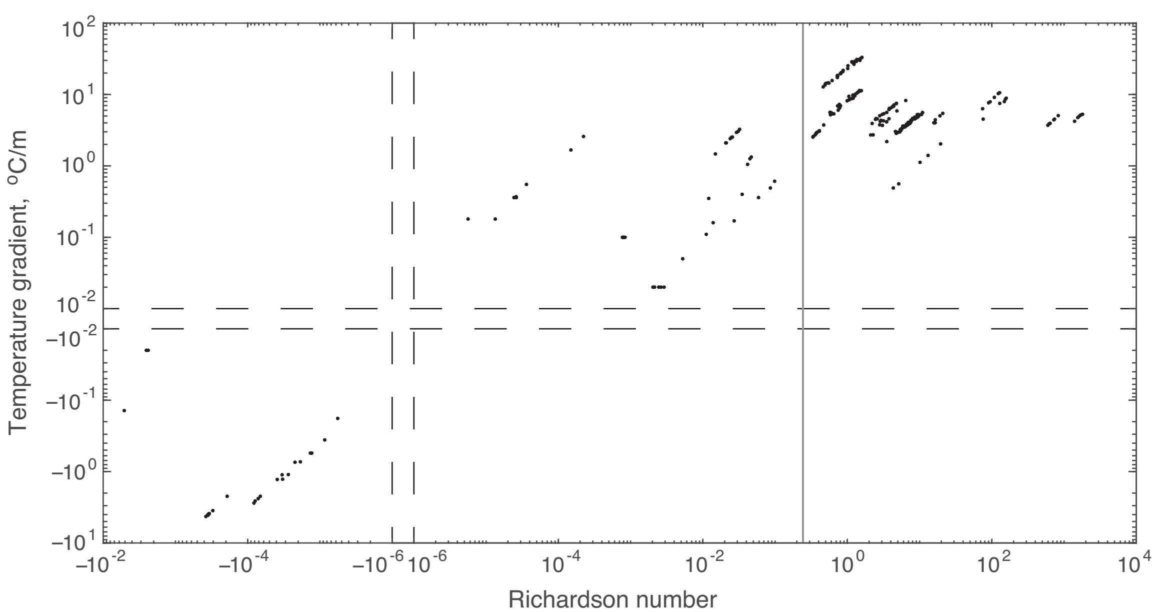

Figure 4. Temperature gradient vs. Richardson number for each column-day at sites with applicable velocity measurements. Positive and negative values of both are shown and separated by dashed lines. Vertical gray line indicates the critical value (0.25) of Richardson number.

The supercritical values of Richardson number, i.e., $\mathbb{R}i > 0.25$, indicate stratification at all of the “true” alcoves at which flow velocities were estimated. This fact, and the lack of a determinative threshold in temperature gradient, led to the inference that all ponds and alcoves (except for W206.6L-Alc) were stratified, and that water in side channels was unlikely to be stratified. For cases of side channels with large cross-sectional area and low enough discharge in the connecting channel, stratification might develop. Following this inference, all column days in all ponds and all alcoves except W206.6L-Alc were included in the calculation and assessment of hyporheic-insolation number. In addition, column-days during low stage at the mouth of W208.5R-SC were also included in hyporheic-insolation number calculation. In total, 445 column-days logged at stratified sites and used to calculate values of hyporheic-insolation number.

Note that stratification does not imply that water near the bed is cool. For some stratified column-days, such as all column-days at W206.0L-Alc, temperatures are generally warmer than in the main channel, less so near the bed: near-bed temperatures are about 0.5 °C warmer than the main channel, while near-surface temperatures are close to 5.5 °C warmer (Figure 4). In contrast, for other stratified column-days, temperatures in the near-bed and near-surface strata straddle the temperatures in the main channel: near-bed temperatures at W207.5-Alc during low river stage are up to 7 °C cooler than the mainstem, while near-surface temperatures are 3.5 °C warmer than the main channel (i.e., spanning a range of 10.5 °C; Figure 4).

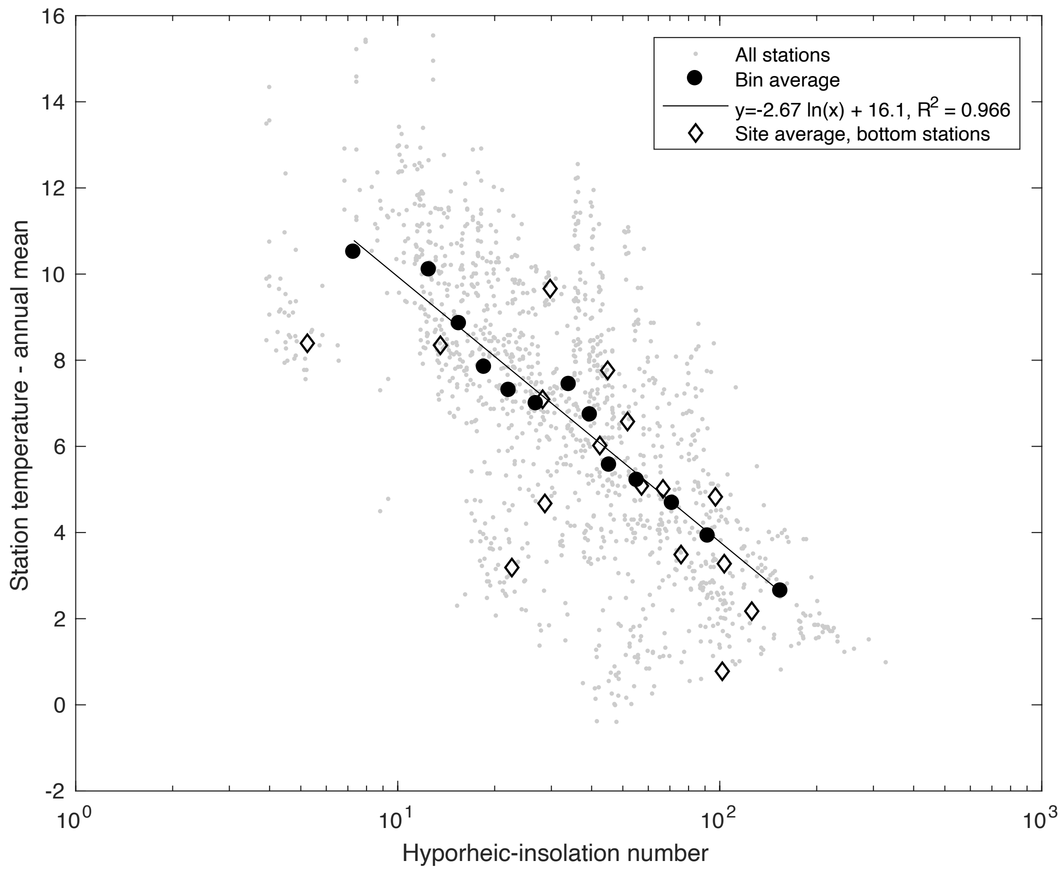

Figure 5. Temperature difference, ΔT_{sa}, vs. hyporheic-insolation number, $\mathbb{H}_{ri}$, for all station-days (bottom, middle, and top) from stratified column-days, 445 station-days in all, as well as bin-averaged values.

4.4.2 Hyporheic-Insolation Number Predicts Measured Temperatures

Temperature measurements for all stratified alcoves and ponds served to ground-truth our calculated values of the hyporheic-insolation number, $\mathbb{H}_{ri}$. We expect temperatures of hyporheic inflows to alcoves, ponds, and side channels, to approach the mean annual stream temperature as subsurface residence times approach one year. To the extent that the hyporheic-insolation number (5) captures this expectation, we expect station-days with greater $\mathbb{H}_{ri}$ to have temperatures closer to the mean annual stream temperature. Therefore, to assess the predictive power of $\mathbb{H}_{ri}$ with measured temperatures, we calculated a temperature difference relative to the annual mean, $\Delta T_{sa} = T_{s,max} - T_a$, for each station-day, where $T_{s,max}$ is daily maximum temperature at a station, and T_a is the annual mean stream temperature for the Harrisburg and

Corvallis reaches, specifically the mean of instantaneous temperatures recorded at 15-minute intervals at the Harrisburg and Albany gages, respectively, during the 2017 calendar year (Table 1).

Hyporheic-insolation numbers that were calculated for all station-days (bottom, middle, and top) at stratified sites, 1335 station-days in all, appear in Figure 6. Given the large amount of scatter, value-pairs for individual station-days are binned according to $\mathbb{H}_{ri}$, so that each bin contains approximately 100 data points, and average values for each bin are also shown in Figure 6. In general, as $\mathbb{H}_{ri}$ increases, temperature difference, ΔT_{sa}, decreases. Bin-averaging markedly reduces the scatter, and the logarithmic fit to the bin-averaged values explains a large fraction of their variance (Figure 6).

Site averages for bottom stations only are also shown. At sites where data were collected both before and after the increase in stage at the beginning of August, site-days before and after the change were treated as different sites for calculation of the site averages. Whereas bin-averaging according to hyporheic-insolation number markedly decreases the scatter about the trend, averaging by site has little effect. The scatter in site averages for bottom stations only is less than the scatter among all station-days, but site averages for middle and top stations are not shown in Figure 6.

4.5 Heat Budgets of Secondary Channel Features

Water temperature at any time reflects the various contributions to the heat budget, changing in response to shifts in the relative magnitudes and directions of heat fluxes. As these magnitudes change cyclically over a 24-hour period, water temperature at a location also changes. To the extent that changes in heat flux are similar from one day to the next, the diel cycle of temperature changes will also be similar, and the salient features of that diel cycle, such as the high and low temperatures and when those extrema occur, may allow us to characterize sites and conditions. That is, differences in typical diel cycles of temperature among sites, and among days with different conditions, do correspond to differences in the heat budget. Inferences based on characteristic diel temperature cycles, such as those shown in Figure 4, may be informative, albeit also speculative without more thorough modeling.

Temperatures in ponds and alcoves generally increased in the downstream direction, but temperatures at two sites decreased downstream. One of these is W206.0L-Alc, which is warm along its whole length, albeit less so at the mouth, and the other is W168.5R-Alc, which shows measurements of cool water temperatures at the mouth (Figure 4). Measurements for column-days at the head of W206.0L-Alc ("the warm one") show water temperatures to be stratified, with bottom-water temperature near the maximum mainstem temperature, barely changing during the day, and reaching a maximum after midnight. In contrast, top-water temperature at the alcove head displays station-day minima and maxima that differ by at least 4°C, with the daily maximum occurring around 13:30. Several processes may be driving these patterns. As the Eastern upstream bank of W206.0L-Alc contained sparse riparian vegetation, stations positioned at the alcove head were exposed to direct sun during hours of maximum isolation. Additionally, the length, L_{ms} used to calculate the mainstem water surface gradient ΔH (Figure 1b) for W206.0L-Alc was small, e.g., 350 m. Different patterns were observed at the mouth of W206.0L-Alc, where field observations noted surface water inflow through a small (width = 1.25 m) lateral channel. Accordingly, column-days at the mouth of this alcove have the smallest temperature gradients of all stratified column-days; the water is only stratified for a few hours per day, and temperatures throughout the column resemble those in the main channel.

Due to inflow of hyporheic discharge with relatively short subsurface residence times, the cooler bottom-water observed at W206.0L-Alc develops but remains warmer than the main channel. During most nights, the water column becomes mixed along the whole length of the alcove, and during the day the water stratifies, first at the head. When stratified, the bottom-water at the head and midpoint heats gradually, and we infer that the lack of mixing between top and bottom strata and the attenuation of the incoming solar radiation in the top stratum mean that the temperature of the bottom stratum is largely determined by conduction of heat from above through molecular diffusion. Due to the relative inefficiency of this mode of heat transfer, the bottom stratum reached its maximum temperature at midnight to 05:00 at the head, where the temperature rose continuously throughout one calendar day of measurements, because the top water did not cool enough at night for mixing to occur.

In contrast, temperatures at the head of W168.5R-Alc (“the cool one”) have large diel fluctuations throughout the column, and the magnitude of those fluctuations decreases as temperatures decrease downstream, especially at the bottom stations. W168.5R-Alc is the only stratified site where water column depth is greatest at the feature mouth, with the bottom-station depth measured to be 1.36 m at the mouth and only 0.46 m at the alcove head. The bottom-station temperatures near the mouth are stable and cool. In contrast to W206.0L-Alc, which seems to cool via mixing with the mainstem at the mouth, the magnitude of hyporheic cooling in W168.5R-Alc is evidently increasing downstream.

Temperatures in W206.6L-Alc and at high stage in W208.5R-SC illustrate the dominance of heat flow by advection and dispersion in cases where the main channel supplies anything more than a relative trickle to the off-channel water body (Figure 4). In these two secondary features, temperatures were nearly identical to those in the main channel. When the flow from the main channel did slow to a trickle, as in W208.5R-SC at low stage, flow at the head and midpoint was well mixed and, due to the water moving slowly through the broad, deep channel, became significantly warmer than in the main channel during the day. At the mouth, the channel was large enough for velocity to slow to the point that buoyant forces led to stratification. However, unlike in alcoves fed by hyporheic flows with long residence times in the subsurface, the bottom stratum of water at the mouth of this side channel had temperatures nearly identical to those in the main channel. Given, first, the warm and well-mixed water upstream of the mouth and, second, our care in locating the near-mouth column far enough upstream to negate the possibility of eddy flow from the main channel affecting temperatures measured in the side channel, this mainstem-like bottom-water stratum must have been, like the alcoves with cool bottom water, sourced by hyporheic flow. However, unlike those alcoves, the hyporheic flow paths feeding the side channel are short, and maximum temperatures in the side channel bottom water lagged those in the mainstem, at W208.6-MC (i.e., approximately 100 m upstream of the inlet to W208.5R-SC), by about two hours.

Temperatures in W207.5L-Alc illustrate the effects of sufficient hyporheic cooling to maintain stratification and cool bottom water throughout the diel cycle and the whole length of the alcove. Both daytime and nighttime bottom-water temperatures increased in the downstream direction, but top-water temperatures decreased (Figure 4). Interestingly, bottom-water temperatures at the mouth of the alcove actually increased during the night, between midnight and sunrise, on two days. In both cases, subtle increases of 0.1–0.2 ^{o}C at the bottom station followed abrupt increases of 1–2 ^{o}C at the middle station, while temperatures at the top station continued to decline. According to meteorological data (crvo), the late-night temperature increases at the middle station coincided with an increase in wind speed and a change in wind direction. In general, temperatures at the middle station at the alcove mouth changed more suddenly than at any other station at W207.5L-Alc. From day to day, and at different times of day, the middle-station temperature at the mouth fluctuated between values within 1–2 °C of either top-station or bottom-station temperatures. These fluctuations imply that the depth of the thermocline was, in general, close to the depth of the middle station, at 0.52 m, but fluctuated between greater and smaller depths, so that relatively subtle variations in the depth of the thermocline produced large temperature swings at the middle station. During the aforementioned windy nights, the subtle increases in bottom-station temperatures may have been due to conductive heat transfer from the warmer water above the thermocline. Relative to water at the mouth, water at the head and midpoint columns was roughly twice as deep. At these deeper locations, middle-station temperatures were consistently similar to the bottom-station temperatures, e.g., within 1 °C. Additionally, both were 7–8 °C cooler than the top-station temperatures (Figure 4). Direct heating during the day was sufficient to increase peak temperatures downstream during the day, although bottom-water temperatures typically peaked shortly after solar noon and heating by conduction from the top layer evidently continued to heat the bottom water during the night. Bottom-water temperatures peaked significantly earlier than temperatures at the top of the water column, and daytime heating from insolation started later and ended earlier at the bottom than at the top. This shortened period of heating is consistent with attenuation of shortwave radiation in the water column. At the surface, relatively weaker insolation in the early morning and late afternoon heated the water, albeit more slowly than when insolation is near its daily maximum. At depth, that weaker insolation was attenuated to the point of insignificant heating by insolation relative to other heat fluxes.

5 Discussion

5.1 Processes controlling water temperature in secondary channel features

Our data and analyses suggest that water temperature in secondary channel features on gravel-bed rivers is controlled by water velocity and hyporheic flow path characteristics. Slow water velocities, such as those found in most alcoves and ponds, allow the water column to reach dynamic stability and become stratified. Likewise, subsurface flow paths that are sufficiently long, have high-permeability substrates, and include preferential hydraulic gradients are likely to be associated with cool hyporheic discharge. Indeed, data from our all of our study sites show stratification and long, high-permeability hyporheic flow paths to be necessary conditions for the presence of cold water.

Water velocity in a channel is related both to the channel's cross-sectional area as well as its volumetric discharge, i.e., the product of channel velocity and the channel cross-sectional area produces the volumetric flow rate. During the summer 2017, reservoir drawdown caused discharge at the USGS Harrisburg Gage to almost double (i.e., 120 m^3/s to 215 m^3/s). Increases were also recorded in discharge measurements (with a flow meter) in the side channel, W208.5R-SC. Measured discharge in the shallow channel connecting the main channel and at the head of the deep section was 0.20 m^3/s and 0.255 m^3/s, respectively, on July 21, prior to the drawdown; on August 9, after the drawdown commenced, measured discharge was 2.33 m^3/s and 2.94 m^3/s, respectively, at the two locations. This 10X increase in discharge was accommodated in the shallow channel by both a 4X increase in the average flow velocity, from 0.13 m/s to 0.54 m/s, as well as a 2.5X increase in cross-sectional area, from 1.63 m^2 to 4.33 m^2. In the deep section of the side channel, the average flow velocity increased from 0.0786 m/s to 0.936 m/s and, like the shallow channel, was associated with an increase in both discharge and cross-sectional area. Figure 5 shows that the stratification that was present for the column located at the mouth of W208.5R-SC before the drawdown became well mixed at high discharge/velocities, with a decrease in $\mathbb{R}i$ from a supercritical values near 0.4 to a subcritical values near 0.004. While a lack of similarly paired flow data from multiple study sites precludes the development of a general relationship between main channel discharge and water velocities observed in secondary channel features, it is clear that an increase in mainstem stage, and the concomitant increases in discharge in side channels can effectively “flip the switch” on stratification, which is, in turn, a necessary condition for development of cool water in secondary channel features. Thus, an increase in discharge aimed at decreasing mainstem water temperature could actually eliminate some cool-water refuges. That said, we should emphasize the “could”: while stratified, the bottom water at the mouth of W208.5R-SC was not cool relative to the main channel, and we did not find that any potential cool-water refuges were eliminated as a result of the August 2017 increase in stage.

Unlike surface water velocity, which can be measured nearly instantaneously, hyporheic flow paths are, by definition, hidden from view and thus more difficult to characterize. While we did not directly measure hyporheic water velocities, hyporheic temperatures, or hyporheic flow path gradients, our study did capture the diel cycle of water temperature in both secondary channel features as well as the main stem. Station-days displaying temperatures buffered in comparison to the amplitude of the main channel are suggestive of long residence times in the hyporheic zone. For example, bottom-water at the head and midpoint of W207.5L-Alc and at the midpoint and mouth of W168.5R-Alc display temperature ranges that are less than half the range observed in the main channel (Figure 4). These measurements suggest that the hyporheic flow paths feeding W207.5L-Alc and W168.5R-Alc are sufficiently long and sufficiently permeable to produce cool hyporheic discharge in large enough quantities to create cool bottom-water in these alcoves.

In addition to temperature measurements, aerial photographs are another tool that support indirect assessment of hyporheic flow path characteristics. Specifically, on gravel-bed rivers, aerial photographs from different years offer information on a site's geomorphic history. These images can indicate dates when a secondary channel feature may have been part of a former main channel path, mark the date riparian vegetation began to emerge on a site, and suggest the upstream terminus of the feature's hyporheic flow paths. Images from different years and at different stages are publicly available on platforms such as Google Earth. Using an aerial photo from June 28, 2017, we created a color-coded map of the thermal regimes throughout the two study reaches for features connected to the main channel at their mouths (Figure 7). All secondary channel temperatures illustrated represent an average of the difference between bottom station and main channel temperatures recorded at the time when the top station of the column reached its daily maximum. For selected features, images from other years, including 1994 and 2003 are also shown. Sites warmer than the main channel, such as W206.0L-Alc, do not have bottom-water temperatures that deviate from main channel temperatures more than 2°C. W206.0L-Alc does not show historical evidence of development of sufficiently long relict channel paths that would allow for cool, buffered hyporheic discharge (Figure 7d). In contrast, colder sites, such as W207.5L-Alc remain connected at high stages to hyporheic flow paths that extend for upwards of 5 km upstream (Figure 7c). Sites like W203.5L-Alc, for which temperature measurements may be found in the supporting information, were along the main channel path of the Willamette as recently as 1994. As a result, hyporheic discharge into W203.5L-Alc likely travels along a preferential hyporheic flow path with high permeability and

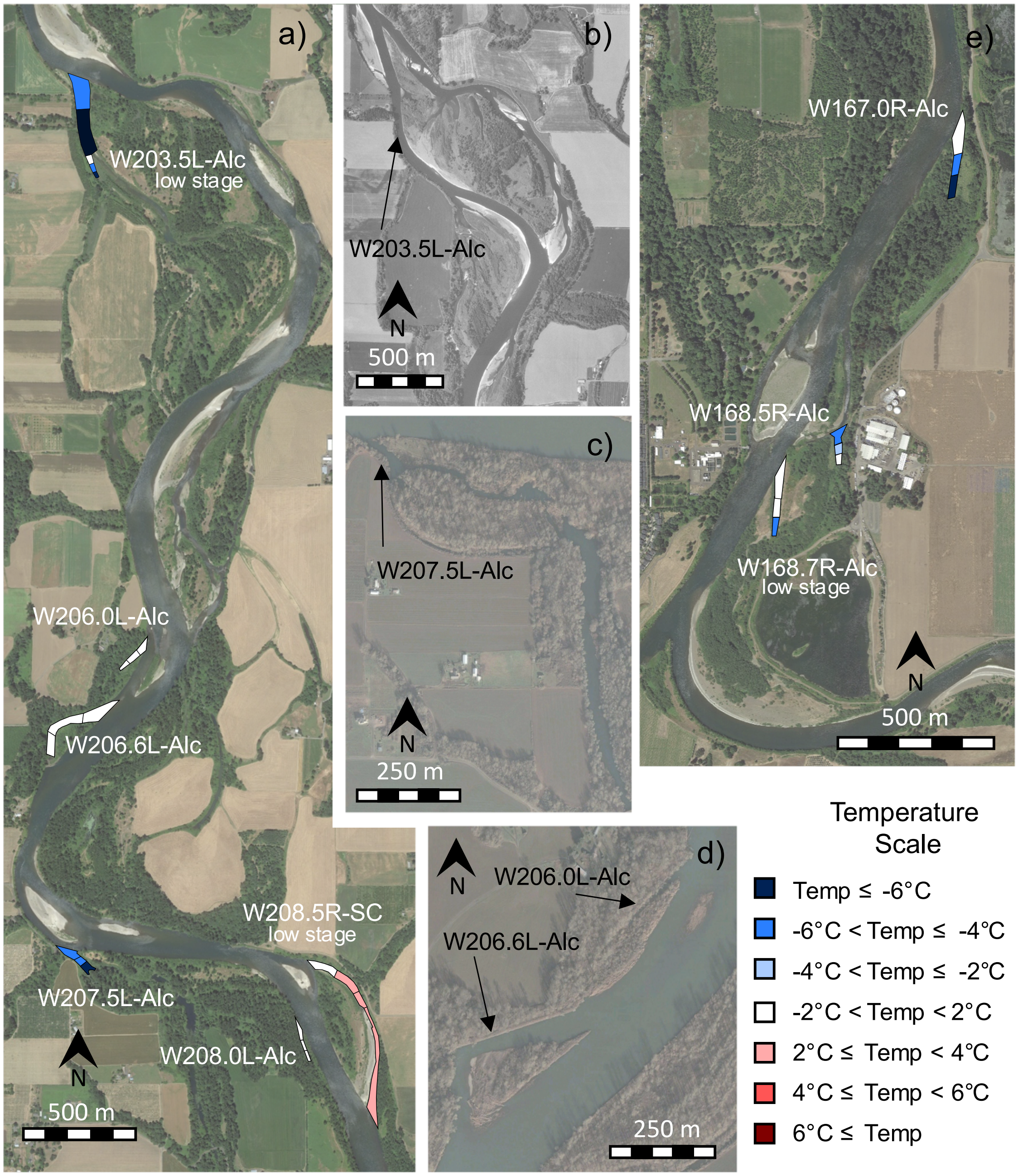

Figure 7. Geographic distribution of averaged near-bed bottom-station temperature measurements for all alcoves and side channel. Harrisburg reach sites appear on a) Google Earth aerial imagery from June 2017. Historical Google Earth aerial imagery from May 1994 shows the main channel flowing through the current location of b) W203.5L-Alc. Google Earth imagery from February 2003 shows high stage channel paths for c) W207.5L-Alc, and d) W206.0L-Alc. Corvallis reach sites appear on e) Google Earth imagery from June 2017. Temperature differences shown are in comparison to the main channel temperature at the time of the near-bed temperature measurements at secondary channel features.

significant length, e.g., 2.9 km (Figure 7b). Taken together, aerial photographs and data from our study suggest that long, abandoned channel paths provide the long residence times and high subsurface flow rates that are both necessary for maintaining cool bottom-water in alcoves and ponds.

While our study did not measure groundwater signature of water in secondary channel features, it is possible that groundwater inputs also control the thermal regimes of stratified alcoves and side channels. In the hyporheic zone, surface water, which is predominantly sourced in the High Cascades and isotopically lighter, can mix with groundwater inputs, which are predominantly sourced from alluvial fans in the valley and isotopically heavier. Past measurements by Hinkle et al. (2001) of stable isotopes in water samples from the mainstem Willamette and secondary channel features have shown that groundwater sources feed some off-channel features, at least at the time of sampling. However, isotopic analyses by Fernald et al. (2006) of samples from the river, alcoves, and shallow wells in the hyporheic zone in the Harrisburg and Corvallis reaches show that isotopic signatures cluster with the river water and appear to rule out inputs from deep groundwater. Additional testing of water samples from study sites could provide additional evidence for the role groundwater plays in shaping the thermal regime of secondary channel features. Even so, whereas groundwater sources may produce cool water in some secondary features, such sources are not necessary to explain the cool water we found, nor do groundwater sources seem particularly likely at any of our sites.

5.2 Characterization of thermal regimes with dimensionless quantities

Thermal regimes of secondary channel features vary not only in time, but also in space. Measurements from the off-channel sites, i.e., alcoves, ponds, and side channels, show that stratification is a necessary, but insufficient, condition for cold water areas. Given stratification, the hyporheic-insolation number is predictive of temperature in these off-channel water bodies.

Of the two dimensionless quantities calculated for secondary channel features, one is descriptive, i.e., Richardson number, and one is predictive, i.e., hyporheic-insulation number. That is, characterization of stratification with the Richardson number is based on temperatures measured in secondary channel features, while our formulation of the hyporheic-insolation number characterizes the relative hyporheic cooling flux based primarily on aerial photographs, publicly available data sets, and literature values. Our $\mathbb{H}_{ri}$ calculations used only one piece of field data, i.e., water depth at the location for which $\mathbb{H}_{ri}$ was calculated. Our own field measurements indicate that empirical relationships between widths and depths of secondary channel features would provide reasonable upper bounds on estimates of depth. While developing such a relationship for a given river would still require collecting data in the field, data from a limited number of sites could provide a means for screening secondary channel features more widely, and based on our understanding of physical processes, features unlikely to contain cool water could be eliminated from further investigation without visiting each site.

The predictive power of hyporheic-insolation number for secondary channel features is technically contingent on stratification, as determined from temperature measurements. However, column-days for alcoves and ponds, i.e., water bodies disconnected from surface flow sources, were generally stratified, and column-days for side channels, i.e., water bodies connected to surface flow sources, were generally unstratified. The exceptions essentially prove the rule: The head of the unstratified alcove was separated from the main channel only by a floating wood jam that permitted flow at rates typical of a side channel. At low water, the head of the stratified side channel was connected to the main channel by a narrow (<10 m), shallow (<0.5 m) channel that carried relatively little flow. In side channels, such as W208.5R-SC at high-stage, and alcoves with insufficient upstream sediment aggradation, e.g., W206.6L-Alc, large inflows generate flow shear sufficient to overwhelm buoyant forces and prevent stratification.

The hyporheic-insolation number predicts the presence of cool water in stratified features on average, but there is substantial scatter in the data for individual station-days. Values of the hyporheic-insolation number were dependent on quantities with significant uncertainties: hydraulic conductivity, insolation attenuation coefficient, mainstem length corresponding to the dominant hyporheic flow path, and local stream gradient. Estimates of the latter two are likely to be within a factor of two or so and are inside the square-root (5), so these are not likely to be large sources of uncertainty. Hydraulic conductivity and attenuation coefficient are more problematic. Hydraulic conductivity, which was estimated from previous measurements and surface vegetation, is well known for its extreme variability. While literature values for K were based on slug tests on a gravel bar on the Harrisburg Reach (Squeochs, 2011), estimation of site age was accomplished through aerial photographs. Only having a known hydraulic conductivity value for a young site does not validate the estimated K values for "developing" and "mature" sites. Attenuation coefficient values increase with the presence of aquatic vegetation in the water column, and uncertainty in this quantity is amplified by an exponential dependence. While our field observations allowed for variation of the attenuation coefficient to reflect the presence or absence of aquatic vegetation, Secchi depth measurements were not collected. Preliminary calculations of hyporheic-insolation number were all based on the same attenuation coefficient: $=1$ m^{-1}. However, data from eutrophic lakes in Oregon include attenuation coefficient values as high as 3.4 m^{-1} (Dodds & Whiles, 2010). This number reflects presence of significant aquatic vegetation. Images of W167.0R-Alc show the presence of dense macrophytes throughout the feature. While not confirmed in the field, site photographs suggest *Ludwigia hexapetala* is present at the upstream end of this site. At W168.5R-Alc, images are unable to sufficiently characterize aquatic vegetation densities. However, field notes record the presence of vegetation at the midpoint and mouth of the feature, indicating a higher attenuation coefficient would likely be appropriate. Additionally, the great depth at the midpoint of W203.5-PR2, i.e., 4.52 m, and clarity of the water suggested an attenuation coefficient of 1 m^{-1} may not be appropriate. Attenuation coefficients for these three features were adjusted to 5 m^{-1}, 2 m^{-1}, and 0.5 m^{-1}, respectively, allowing hyporheic-insolation numbers calculated to successfully characterize the temperatures recorded at each site. Decreasing these uncertainties further could provide a clearer picture. For example, determination of attenuation coefficients with depths recorded by a Secchi disk would likely reduce scatter. Even so, the logarithmic fit to bin-averaged station-day $\mathbb{H}_{ri}$ points had R^2= 0.97.

5.3 Relationship between thermal regimes and habitat quality

Water temperature is one of the defining habitat characteristics for anadromous cold water fishes. At different life stages, anadromous salmonids use habitats from the ocean to river headwaters (Wilson, 1997). Thermal conditions directly relate to physiology and disease resistance of native cold-water fishes. For example, imperiled spring Chinook Salmon achieve maximum growth at 14.8 °C and experience lethal conditions when temperatures exceed 25.1°C (McCullough, 1999). The upper Willamette River provides important rearing habitat for juvenile spring Chinook Salmon, as well as serving as a corridor for out-migrating smolts that are leaving freshwater to rear in estuary and marine environments (Schroeder et al., 2012). Thus, the Willamette must be able to provide habitat below critical temperature limits coincident with the adult spawning migration, as well as for the rearing and outmigration of juveniles.

Temperature standards of the Oregon Department of Environmental Quality categorize areas that are at least 2 °C cooler than the mainstem during the time of the mainstem daily maximum as cold water refugia for salmonids. Out of our seven stratified alcoves, five have at least one location with water temperature measurements that are at least 2 °C cooler than the mainstem at the time of the daily maximum temperature: W207.5L-Alc, W203.5L-Alc, W168.7R-Alc, W168.5R-Alc, and W167R-Alc. However, legally defined cold water refuges do not necessarily provide all of the ecosystem services required by cold water fishes such as spring Chinook Salmon. In particular, the ODEQ standard defines an area that is cooler relative to the mainstem as a thermal refuge, even if the temperature of the secondary channel feature still exceeds physiological limits for cold water fishes.

Adequate levels of dissolved oxygen are also an important habitat quality for fishes. For salmonids, dissolved oxygen levels may partially restrict suitable cold water habitats (Ebersole et al., 2003). Dissolved oxygen levels below 6.0 mg/L have been identified as lethal to salmonids (Davis, 1975). Accordingly, ODEQ regulations for dissolved oxygen in “water bodies...providing cold-water aquatic life,” including the Willamette River Basin, outline “6.0 mg/L as an absolute minimum” (ODEQ, 2007).

Biologically relevant cold water refuges provide not only cold water but also sufficient dissolved oxygen. Two of the stratified sites cooler than the main channel, W207.5L-Alc and W203.5L-Alc, provide at least 6.0 mg/L at near-bed depths. However, the cool areas of W168.7R-Alc and W168.5R-Alc provide <2 mg/L of DO just above the bed. While these two alcoves meet the legal definition of a cold water refuge, the ecosystem services they provide may not be biologically sufficient for salmonids. While DO point measurements were not taken at W167R-Alc, the density of macrophytes may actually suggest the presence of anoxic conditions.

If the observed aquatic vegetation includes *Ludwigia hexapetala*, DO levels may be below 6.0 mg/L. Because Ludwigia is an emergent aquatic plant, its leaves exchange gases with the atmosphere rather than the water column (Rose & Crumpton, 1996). Atmospheric exchange results in depleted levels of dissolved oxygen in the water itself. Thus, while secondary channel features with *L. hexapetala* may meet the legal definition of a cold water refuge, these sites are not biologically relevant for salmonids.

Hyporheic exchange affects both the temperature and the dissolved oxygen concentration of water flowing through the subsurface. DO levels of hyporheic water are lower than those of river water (Fernald et al., 2006). As a result, hyporheic discharge in secondary channel features is often anoxic. Residence times longer than 6.9 hours are associated with net anoxic conditions and anaerobic microbial processes (Zarnetske et al., 2011). While hyporheic discharge may be cool, it may not provide suitable habitat for cold water fishes. In our study, the two stratified alcoves that are not biologically relevant, W168.7R-Alc and W168.5R-Alc, have the lowest DO readings at the locations with the coolest temperatures. Both of these water quality parameters may be the result of long subsurface flow paths and long residence times in the hyporheic zone.

Dissolved oxygen values in this study are based on point measurements. Often, a single measurement was taken at each column and at each station for each site. While attempts were made to position the instrument at a location that corresponded to a station at a given column before readings were recorded, there was likely measurement error. For example, some near-bed measurements may have recorded values taken while the DO probe was submerged in bed sediment, resulting in especially low readings. Deploying a DO probe to record continuous measurements at known station elevations in the water column would provide more robust data to inform habitat quality assessments.

5.4 Restoration Implications

The ability to identify potential cold water areas in large gravel-bed rivers holds implications for successful restoration of ecosystem services in modified basins. Required inputs for the hyporheic-insolation number can be obtained from: (a) aerial photographs, (b) stream gages, (c) meteorological stations, (d) literature values, and (e) water depth measurements. The values used to calculate the hyporheic-insolation number for this study were based on aerial images from Google Earth, water temperature data collected in the main channel at USGS gages 14166000 (Willamette River, Harrisburg, OR) and 14174000 (Willamette River, Albany, OR), daily solar radiation data from USBR AgriMet Weather Station (Corvallis, Oregon), published values of slope and hydraulic conductivity for the upper Willamette (Dykaar & Wigington, 2000; Fernald et al., 2006; Squeochs, 2011), and values for attenuation coefficient of lakes in Oregon (Dodds & Wiles, 2010). The only field measurements required were the depths of secondary channel features.

Preliminary classification of thermal regimes of secondary channel features should group all active side channels into a single class. Stratification is a necessary condition for cold water areas found in secondary channel features. Inflow of surface water in the side channel, W208.5R-SC, caused mixing throughout the water column, especially during high river stage. Alcoves disconnected from the main channel at the upstream end by large wood rather than gravel deposits should also be classified as de-stratified, i.e., W206.6L-Alc.

While dimensionless ratios such as the hyporheic-insolation number capture contributions of hyporheic discharge and solar heating, other drivers are known to affect the thermal regime of secondary channel features. First, the river stage of the main channel impacts surface water inflow into sites. This in turn, impacts presence of stratification of the water column (e.g., W208.5R-SC, Figure 4). Second, beaver ponds influence hydrologic processes downstream of dams during both low-flow and peak flow periods (Westbrook et al., 2006). Beaver ponds were found upstream of three of the alcoves in this study, W206.6L-Alc, W203.5L-Alc, and W168.5R-Alc, and likely influenced hyporheic exchange in these floodplain areas. Furthermore, gravel pits, which form man-made ponds, were also adjacent to all three alcoves in the Corvallis study reach. While impacts of such human floodplain modifications on hyporheic exchange and water table levels have not been studied for the upper Willamette, it is possible gravel ponds influence the thermal regime of nearby secondary channel features. Finally, as already touched upon, contributions from groundwater may shape thermal regimes in large gravel-bed rivers. Specifically, groundwater seeps may contribute to cold near-bed water temperatures measured in stratified alcoves and ponds. The presence of these seeps might not depend on characteristics that produce large values of hyporheic-insolation number. Further isotopic analysis of study sites could provide data to allow for characterization of the role groundwater plays in shaping the thermal regime of secondary channel features.

6 Conclusions

Rivers such as the Willamette continue to have mainstem temperatures too warm for cold water fishes during periods of rearing and migration. However, the likelihood of addressing this challenge by significantly cooling the main channel is small. Instead, we are working to advance our understanding of processes controlling thermal regimes of secondary channel features along gravel-bed rivers. With the predictive hyporheic-insolation number, the thermal regime of secondary channel features may be characterized remotely, requiring neither extensive modeling nor widespread field data collection. This dimensionless ratio may be able to increase our ability to locate and enhance such features across a floodplain.

Water velocity and site geomorphic history control the thermal regimes of secondary channel features on the upper Willamette River. Features that provide thermal refuges to cold water fishes are characterized by stratification and by long, high-permeability subsurface flow paths. In other words, stratification is a necessary yet insufficient condition for cold water areas. In this study, the side channel and alcove with significant surface water flow were well-mixed and were not cooler than the mainstem. Likewise, the alcoves and ponds that were warmer than the mainstem, while stratified, had hyporheic flow paths that were either short in length or had low values of hydraulic conductivity, or both. Even at sites cooler than the mainstem, dissolved oxygen measurements indicate some cold water may be too anoxic for fish. Ultimately, both temperature and fish use data are needed to paint a complete picture of habitat quality in secondary channel features. Even so, this study provides empirical evidence that only stratified alcoves and ponds with long, high-permeability hyporheic flow paths are cooler than the well-mixed mainstem.

Acknowledgements

This research was supported by NSF STEM award 1153490, Geological Society of America's Graduate Student Research Grants, and the Kenneth H. Crandall Memorial Grant from the American Association of Petroleum Geologists. Mary Santlemann and Elizabeth Gombert provided invaluable support for project recommencement following a period of leave for one of the authors. Morgan Tholl and Barry Gombert provided field data collection support. Data for this project is available online through the Consortium of Universities for the Advancement of Hydrologic Science (Gombert et al., 2020).

References

Arrigoni, A. S., Poole, G. C. , Mertes, L. A. K., O'Daniel, S. J., Woessner, W. W., & Thomas, S. A. (2008). Buffered, lagged, or cooled? Disentangling hyporheic influences on temperature cycles in stream channels. *Water Resources Research 44*(9), 1-13. https://doi.org/10.1029/2007WR006480

Arscott, D.B., Tockner, K., & Ward, J.V. (2002). Thermal heterogeneity along a braided floodplain river (Tagliamento River, northeastern Italy). *Canadian Journal of Fisheries and Aquatic Sciences 58*(12), 2359-2373. https://doi.org/10.1139/f01-183

Beschta, R.L., & Taylor, R.L. (1988). Stream temperature increases and land use in a forested Oregon watershed. *Water Resources Bulletin*, *24*, 19–25. https://doi.org/10.1111/j.1752-1688.1988.tb00875.x

Brett, J. R. (1971). Energetic responses of salmon to temperature. A study of some thermal relations in the physiology and freshwater ecology of sockeye salmon (Oncorhynchus nerkd). *American zoologist*, *11*(1), 99-113. https://doi.org/10.1093/icb/11.1.99

Buckingham, E. (1914). On physically similar systems; illustrations of the use of dimensional equations. *Physical review*, *4*(4), 345. https://doi.org/10.1103/PhysRev.4.345

Burkholder, B. K., Grant, G. E., Haggerty, R., Khangaonkar, T., & Wampler, P. J. (2008). Influence of hyporheic flow and geomorphology on temperature of a large, gravel-bed river, Clackamas River, Oregon, USA. *Hydrological Processes, 22*, 941– 953. https://doi.org/10.1002/hyp.6984

Caissie, D. (2006). The thermal regime of rivers: a review. *Freshwater biology, 51*(8),1389-1406. https://doi.org/10.1111/j.1365-2427.2006.01597.x

Cluis, D. A. (1972). Relationship between stream water temperature and ambient air temperature: A simple autoregressive model for mean daily stream water temperature fluctuations. *Hydrology Research*, *3*(2), 65-71. https://doi.org/10.2166/nh.1972.0004

Cole, T.M., & Wells, S. A. (2006). CE-QUAL-W2: A two-dimensional, laterally averaged, Hydrodynamic and Water Quality Model, Version 3.5. (Instruction Report EL-06-1). Vicksburg, MS: U.S. Army Engineering and Research Development Center.

Davis, J. C. (1975). Minimal dissolved oxygen requirements of aquatic life with emphasis on Canadian species: a review. *Journal of the Fisheries Board of Canada, 32*(12), 2295-2332. https://doi.org/10.1139/f75-268

Dodds, W. K., & Whiles, M.R. (2010). *Freshwater ecology: concepts and environmental applications*. Burlington, MA: Academic Press.

Dugdale, S.J. (2016). A practitioner's guide to thermal infrared remote sensing of rivers and streams: recent advances, precautions and considerations. *Wiley Interdisciplinary Reviews: Water, 3,* 251–268. https://doi.org/10.1002/wat2.1135

Dykaar, B. B. & Wigington, P. J. (2000). Floodplain formation and cottonwood colonization patterns on the Willamette River, Oregon, USA. *Environmental Management*, *25*(1), 87-104. https://doi.org/10.1007/s002679910007

Ebersole, J. L., Liss, W. J., & Frissell, C. A. (2003). Thermal heterogeneity, stream channel morphology, and salmonid abundance in northeastern Oregon streams. *Canadian Journal of Fisheries and Aquatic Sciences*, *60*(10), 1266-1280. https://doi.org/10.1139/f03-107

Elliot, J.M. & Hurley, M. A. (1997). A functional model for maximum growth of Atlantic Salmon parr, Salmo salar, from two populations in northwest England. *Functional Ecology 11,* 592-603. https://doi.org/10.1046/j.1365-2435.1997.00130.x

Fernald, A. G., Landers, D. H., & Wigington, P. J. (2006). Water Quality Changes in Hyporheic Flow Paths Between a Large Gravel Bed River and Off-Channel Alcoves in Oregon, USA. River Research and Applications *22*(10), 1681-1794. https://doi.org/10.1002/rra.961

Fullerton, A. H., Torgersen, C. E., Lawler, J. J., Steel, E. A., Ebersole, J. L., & Lee, S. Y. (2018). Longitudinal thermal heterogeneity in rivers and refugia for coldwater species: effects of scale and climate change. *Aquatic sciences*, *80*(1), 3. (2018). https://doi.org/10.1007/s00027-017-0557-9

Gombert, C.E., Lancaster, S.T., Flitcroft, R.L, & Grant, G.E. (2020). *Upper Willamette Water Temperature Data in Secondary Channel Features, 2017* [Data file]. *http://data.cuahsi.org*

Hannah, D.M. & Garner, G. (2015). River water temperature in the United Kingdom: Changes over the 20th century and possible changes over the 21st century. *Progress in Physical Geography: Earth and Environment, 39*(1): 68-92. https://doi.org/10.1177/0309133314550669

Hinkle, S. R., Duff, J. H., Triska, F. J., Laenen, A., Gates, E. B., Bencala, K. E., Wentz, D.A., & Silva, S. R. (2001). Linking hyporheic flow and nitrogen cycling near the Willamette River—a large river in Oregon, USA. *Journal of Hydrology*, *244*(3-4), 157-180. https://doi.org/10.1016/S0022-1694(01)00335-3

Hulse, D., Gregory, S.V., & Baker, J. (Eds.). 2002. *Willamette River Basin Planning Atlas: Trajectories of Environmental and Ecological Change.* Corvallis, Oregon: Oregon University Press.

Isaak, D. J., Young, M. K., Nagel, D. E., Horan, D. L., & Groce, M. C. (2015). The cold-water climate shield: delineating refugia for preserving salmonid fishes through the 21st century. *Global Change Biology*, *21*(7), 2540-2553. https://doi.org/10.1111/gcb.12879

Jackson, F.L., Malcolm, I.A., & Hannah, D.M. (2016). A novel approach for designing large-scale river temperature monitoring networks. *Hydrology Research 47* (3): 569–590. https://doi.org/10.2166/nh.2015.106

Johnson, S. L. (2004). Factors influencing stream temperatures in small streams: substrate effects and a shading experiment. *Canadian Journal of Fisheries and Aquatic Sciences*, *61*(6), 913-923. https://doi.org/10.1139/f04-040

Johnson, S. L. & Jones, J. A. (2000). Stream temperature responses to forest harvest and debris flows in western Cascades, Oregon. *Canadian Journal of Fisheries and Aquatic Sciences*, *57*(S2), 30-39. https://doi.org/10.1139/f00-109

Keefer, M. L. & Caudill, C. C. (2015). Estimating thermal exposure of adult summer steelhead and fall Chinook salmon migrating in a warm impounded river. *Ecology of freshwater fish*, *25*(4), 599-611. https://doi.org/10.1111/eff.12238

McCullough, D. A. (1999). A review and synthesis of effects of alterations to the water temperature regime on freshwater life stages of salmonids, with special reference to Chinook salmon. (Report No. 910-R-99-010) U.S. Environmental Protection Agency. https://nepis.epa.gov/Exe/ZyPDF.cgi/P1004JG1.PDF?Dockey=P1004JG1.PDF

Merck, M. F. & Neilson, B. T. (2011). Modelling in-pool temperature variability in a beaded arctic stream. *Hydrological Processes, 26*(25), 3921-3933. https://doi.org/10.1002/hyp.8419

O'Connor, J. E. (2001). Origin, extent, and thickness of Quaternary geologic units in the Willamette Valley, Oregon. (Professional Paper No. 1620). U.S. Geological Survey. https://pubs.usgs.gov/pp/1620/pdf/pp1620.pdf

ODEQ. (2007). 340-041-0028: Water Quality Standards: Beneficial Uses, Policies, and Criteria for Oregon-- Temperature. Ed. Oregon Department of Environmental Quality. https://secure.sos.state.or.us/oard/viewSingleRule.action?ruleVrsnRsn=244176

Peixoto, J. P. & Oort, A. H., 1992. *Physics of Climate*. New York: American Institute of Physics.

Poole, G. C. & Berman, C. H. (2001). An ecological perspective on in-stream temperature: natural heat dynamics and mechanisms of human-caused thermal degradation. *Environmental management*, *27*(6), 787-802. http://dx.doi.org/10.1007/s002670010188

Rose, C. & Crumpton, W. G. (1996). Effects of emergent macrophytes on dissolved oxygen dynamics in a prairie pothole wetland. *Wetlands*, *16*(4), 495-502. https://doi.org/10.1007/BF03161339

Rumble, J.R. (Ed.). (2018). *CRC Handbook of Chemistry and Physics, 99th Edition.* CRC Press. http://hbcponline.com

Squeochs, G. (2011). *Heat fluxes in the hyporheic zone of a gravel bar on the Willamette River, Oregon* (Master's thesis). Retrieved from OSU Scholar's Archive, (https://ir.library.oregonstate.edu/concern/graduate_thesis_or_dissertations/5d86p3452). Corvallis, OR: Oregon State University.

Steel, E. A., Beechie, T. J., Torgersen, C. E., & Fullerton, A. H. (2017). Envisioning, quantifying, and managing thermal regimes on river networks. *BioScience*, *67*(6), 506-522. https://doi.org/10.1093/biosci/bix047

Stefan, H. G. & Preud'homme, E. B. (1993). Stream temperature estimation from air temperature. *Journal of the American Water Resources Association*, *29*(1), 27-45. https://doi.org/10.1111/j.1752-1688.1993.tb01502.x

Torgenson, C.E., Ebersole, J.L., & Keenan, D.M. (2012). Primer for Identifying Cold-Water Refuges to Protect and Restore Thermal Diversity in Riverine Landscapes. (Report No. 910-C-12-001). U.S. Environmental Protection Agency. //pubs.er.usgs.gov/publication/70037945

Vannote, R.L., Minshall, G.W., Cummins, K.W., Sedell, J.R., & Cushing, C.E. (1980). The river continuum concept. *Canadian Journal of Fisheries and Aquatic Science 37*, 130-137. https://doi.org/10.1139/f80-017

Wallick, J.R., Grant, G.E., Lancaster, S.T., Bolte, J.P., & Denlinger, R.P. (2007). Patterns and Controls on Historical Channel Change in the Willamette River, Oregon, USA. In Gupta, A. (Ed.) *Large rivers: geomorphology and management* (pp. 491-516). West Sussex, England: John Wiley & Sons.

Wallick, J. R., Jones, K. L., O'Connor, J. E., Keith, M. K., Hulse, D., & Gregory, S. V. (2013). Geomorphic and vegetation processes of the Willamette River floodplain, Oregon-Current understanding and unanswered questions. (Open File Report 2013-1246). U.S. Geological Survey. https://doi.org/10.3133/ofr20131246

Wallick, J.R., Lancaster, S.T., & Bolte, J.P. (2006). Determination of bank erodibility for natural and anthropogenic bank materials using a model of lateral migration and observed erosion along the Willamette River, Oregon, USA. *River Research and Applications 22*(6) 631-649. https://doi.org/10.1002/rra.925

Ward, J.V. (1985). Thermal characteristics of running rivers. *Hydrobiologia 125*, 31–46. https://doi.org/10.1007/BF00045924

Westbrook, C. J., Cooper, D. J., & Baker, B. W. (2006). Beaver dams and overbank floods influence groundwater–surface water interactions of a Rocky Mountain riparian area. *Water Resources Research, 42*(6). https://doi.org/10.1029/2005WR004560

Wilson, M. F. (1997). Variation in salmonid life histories: patterns and perspectives. (Research Paper PNW-RP-498). Portland, OR: U.S. Department of Agriculture, Forest Service, Pacific Northwest Research Station. https://doi.org/10.2737/PNW-RP-498

Zarnetske, J. P., Haggerty, R., Wondzell, S. M., & Baker, M. A. (2011). Dynamics of nitrate production and removal as a function of residence time in the hyporheic zone. *Journal of Geophysical Research: Biogeosciences, 116(G1)*. https://doi.org/10.1029/2010JG001356